ADELEv2017

A Software for

Age **DE**termination based on **L**uminescence and **E**lectron spin resonance

Manual & Tutorial

Mohorn, 01.03.2019

1. Manual

1.1. Introduction

ADELEv2017 is a software developed for the age determination by dosimetric methods like luminescence or e.s.r. dating. In comparison to other approaches the commonly used concept of constant dose rates and other constant outer parameters is given up. Instead of the time dependence of the dose accumulated by a grain is calculated and compared to the measured palaeodose. This procedure allows the age determination e.g. in environments with changing overburden, varying moisture and time dependent radioactive disequilibria.

The Java based software is platform independent and can thus be used under different operating systems. The functionality of **ADELEv2017** is a relaunch of the older ADELE version presented in 2005 ([1], [2]) but implemented by a totally new developed program code.

ADELEv2017 creates files with the extension "adx". All input data as well as the results of the age determination are stored with these *.adx files.

Depending on the knowledge and experience of the user, **ADELEv2017** can be performed in a *Standard mode* as well as in an *Expert mode*. The latter mode allows the introduction of time dependent moisture and burial depth, the investigation of layered deposition condition as well as the consideration of radioactive disequilibria in the ^{238}U decay series.

ADELEv2017 can be purchased from the ADD ideas Dr. Detlev und Albrecht Degering GbR, Germany via the website https://add-ideas.com/.

*Note: **ADELEv2017** is still actively developed. This means, that there will be regular updates and the functionally is still being extended. New functions are added with every release. In some cases, this also means that some functions are not working as they should (yet). If you feel you discovered such a function, feel free to contact us at kontakt@adele.ad5-ar.de.*

1.2. Installation

A precondition of the operation of **ADELEv2017** is a working Java Runtime Environment (JRE). The Java trademark is owned by the Oracle Corporation which distributes the JRE at java.com (free available). The process of installing a JRE is described at this website. Although untested, **ADELEv2017** might work with alternative JREs, like OpenJDK.

After the successful installation of the JRE, **ADELEv2017** is easily started by double clicking on the program icon in the start menu. If you chose to create a shortcut on your Desktop during the installation process, double-clicking on the icon will also open the program. In the case of installation problems one should consult our service at kontakt@adele.ad5-ar.de.

1.3. Licensing and license activation

To run **ADELEv2017**, you need to purchase a license. If you are interested in purchasing a license, please contact us at lizenz@adele.ad5-ar.de.

Once you have purchased a license, you receive a serial number. This serial number needs to be provided to the activation wizard, which will guide you through the activation process.

1.4. Standard mode

At the first time, the program starts a window in the *Standard mode* which already contains all functions necessary for a common age determination. The additional abilities and functions of the *Expert mode* are described in chapter 1.5.

The general visual structure of **ADELEv2017** does not depend from the chosen mode. It includes the Menu / Icon bar in the upper part of the window, the Workspace window at the left side, the Data window in the middle and the Results / Report window at the right (Figure 1). The horizontal width of the windows can be altered by shifting the vertical frame lines with the computer mouse.

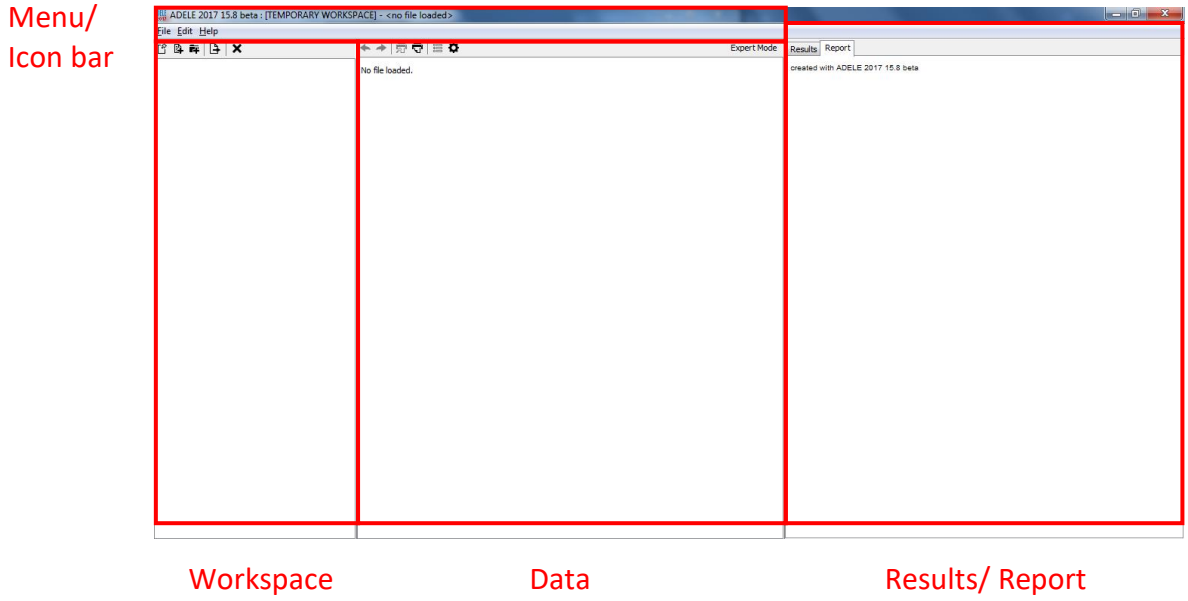

Figure 1 General window structure of **ADELEv2017**.

1.4.1. Menu/ Icon bar

The upper part of the bar contains the *File*, *Edit* and *Help* Menu.

The *File* menu contains all common operations for the Workspace window like *New*/*Open*/*Save*/*Close*. Furthermore, *.adl files created by the older ADELE version from 2005 can be opened using the *Import* command. *Print* refers to the output of the content of the Results / Report window. The user can select which of the Results / Report tabs should be printed. Finally, this menu also includes the *Exit* command.

Edit contains the *Undo*/*Redo*/*Delete* commands.

Some of these commands are also accessible by direct clicking on the icons in the lower part of the menu bar.

1.4.2. File tree window

The file tree shows all files opened in **ADELEv2017**. Folders or "nodes" can be defined in the tree for the sake of a better clarity. The *Insert* / *Remove* commands in this window act only on the nodes. The user may change the description of the folders by pressing the function key F2.

*Note: A fully functional file tree will be implemented in a future version of **ADELEv2017**.*

Each file is labeled in the file tree first by the sample description (see 1.4.3, General data) and by the file name. The position in the tree structure can be altered by dragging the nodes to the new position. Unsaved changes in the file data are indicated by an asterisk.

An example of an file tree is shown in Figure 2.

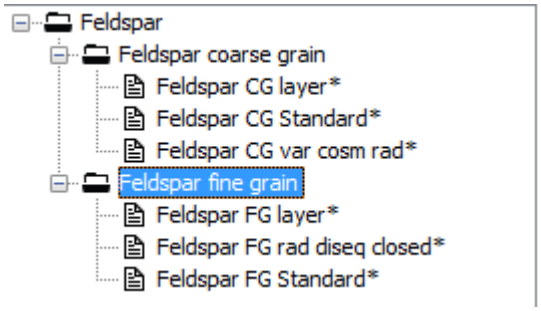

Figure 2 Example of the file tree structure

1.4.3. Data window

The Data window allows the input of all relevant data by the user. Clicking into a frame allows the entry of data. Alternatively, the Tab key can be applied for skipping between the input frames. The input is not sensitive to the used decimal separator i.e. both notations “xxx.xx” and “xxx,xx” can be typed but are displayed in both case as “xxx.xx”.

The data input is structered by the sub-frames *General data*, *Grain properties*, *Cosmic radiation*, *Internal dose* and *External dose*. Each of the sub-frame is opened or closed by clicking on the header lines shown in Figure 3. The meaning of the individual input data is shortly described hereafter.

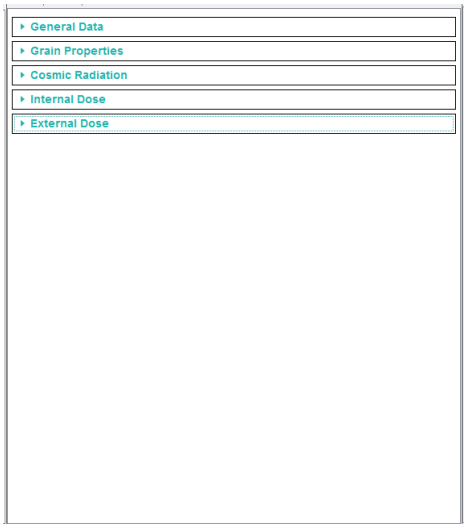

Figure 3 Data window, all sub-frames closed.

General data

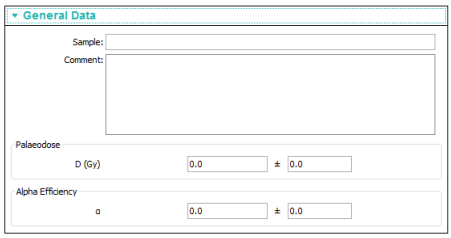

Figure 4 General data frame, as shown when opening a new project.

Sample stands for the user's short name of the sample or another distinctive description. This name will also be displayed as the project's name in the Workspace window.

Comment includes any further text information which is worth remembering or necessary for a detailed understanding of the applied model.

Palaeodose D is the dose value in Gy and its uncertainty determined from the dosimetric procedure (optically stimulated luminescence [OSL], thermoluminescence [TL], electron spin resonance [e.s.r.] etc.). Note that the frequently used term "equivalence dose" is not used in **ADELEv2017** (cf. 2.1.1, *Decay types and radiation characteristics*)

Alpha Efficiency is the also called a-value described in chapter 2.2.3 with its uncertainty.

Grain properties

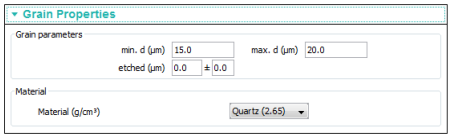

Figure 5 Grain properties frame, as shown when opening a new project.

Grain parameters describes the properties of the dated grains as a whole. "min d" and "max d" mean the minimum and maximum grain diameter in µm, respectively, as a result e.g. of a sieving procedure. If the grains were etched subsequently to remove the surface layer exposed to the α-dose (cf. chapter 2.2.2), the estimated thickness of the etched layer with its uncertainty should be entered in the "etched"frame. It is not possible to enter a value smaller than half of the minimum grain diameter. The case of etching prior to sieving is treated in the expert mode, see 0.

Material is the selection of the dated material: "Quartz" or "Feldspar". If the polymineralic fine grain fraction was investigated one should select "Feldspar".

Cosmic radiation (see also chapter 2.1.2)

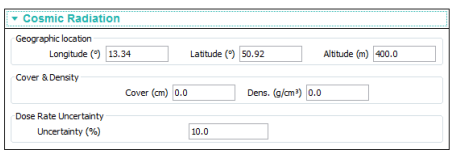

Figure 6 Cosmic radiation frame, as shown when opening a new project.

Geographic location defines the position of sampling with respect to: *Longitude* (eastward - positive, westward - negative), *Latitude* (North - positive, South - negative) and *Altitude* (elevation in meters a.s.l.).

Cover & Density describes the overburden: *Cover* means its thickness in cm, *Dens.* its mean bulk density in $g \cdot cm^{-3}$

Dose Rate Uncertainty refers to the uncertainty of the cosmic dose rate; because of past variations of the cosmic particle flux it is recommended to choose a value not smaller than 10 % (see 2.1.2)

Internal dose

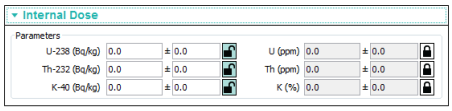

Figure 7 Internal dose frame, as shown when opening a new project.

Parameters requires the entry of the radionuclide content with uncertainty of the dated material itself, either as specific activity in $Bq \cdot kg^{-1}$ or as concentration in ppm. Switching is achieved by clicking on the padlock symbol. Considered are the ^{238}U and ^{232}Th decay series in equilibrium as well as ^{40}K. Note that a potassium content of (12.5 ± 0.5) % is often used for dating K-feldspars; but this value may vary for feldspars of different origin (see the remark in 2.2.4). For the correct use of the term "internal dose" in the dating of potsherds etc. see the discussion in 2.2.2.

External dose

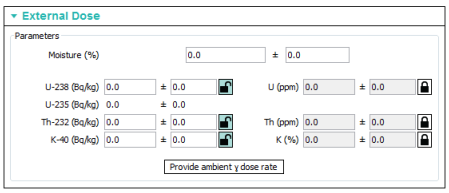

Figure 8 External dose frame, as shown when opening a new project.

Parameters is similarly structured as for *Internal dose* but refers to the material surrounding the dated objects. The specific activity of ^{235}U is calculated from the natural ^{235}U / ^{238}U activity ratio.

Additionally an information about the *Moisture* and its uncertainty is requested. Please bear in mind the definition of this parameter given in 2.2.2.

Provide ambient dose rate is a button which allows the user input of an in-situ value of the ambient γ dose rate; as e.g. determined from NaI(Tl) detector measurements. In this case only α and β dose rates are calculated from the given contents of ^{238}U, ^{232}Th and ^{40}K, the γ dose rate is replaced in the calculation by D_γ (unit $\mu Gy \cdot a^{-1}$). Note that this function is not available in the *Expert mode*.

1.4.4. Results / Report window

The Results / Report window summarises input data as well as important results of the calculation procedure. The presented data will be refreshed after each new input, so the influence of parameter variations on the age value are instantly displayed. For

documentation these pages can be printed using the *Print* commands from the Menu / Icon bar.

The *Report* data include all inputs made in the Data window as well as the main result of the calculation, the age value.

Results shows beside the age result the total dose rate as well as their contributions from cosmic, internal and external radiation. The latter two are divided into the alpha(eff), beta and gamma component whereas alpha(eff) means the effective alpha dose rate taking into account the a-value (see chapter 2.2.3). Remember that the internal gamma dose rate is zero because of the negligible grain diameter compared to the gamma radiation range (correction term $\phi^{\gamma} = 0$, see 2.2.2).

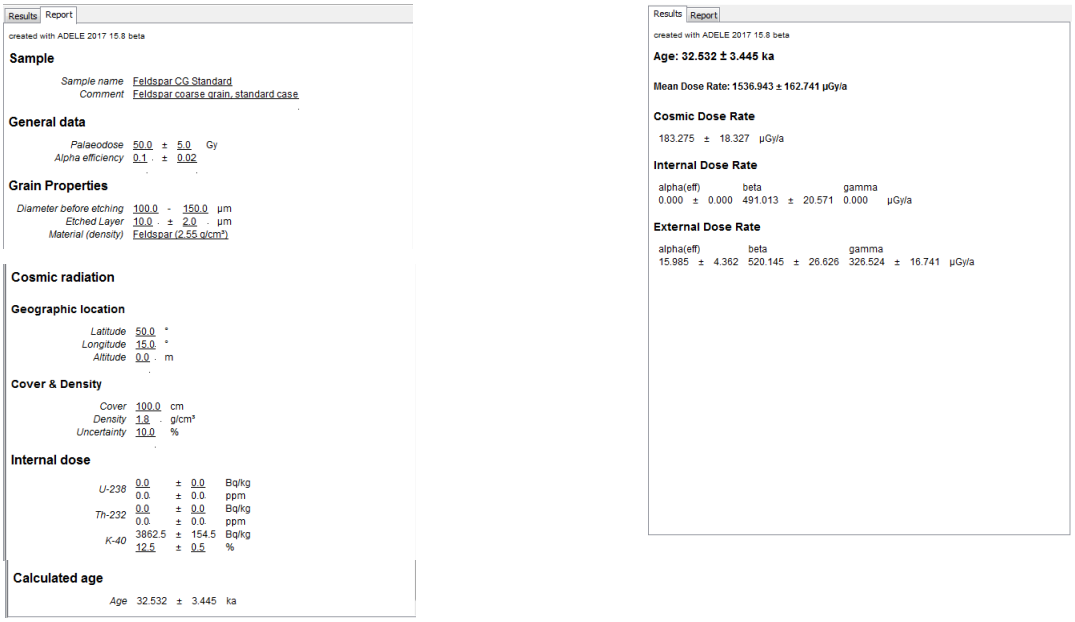

Figure 9 Examples of the displayed data in the Report (left) and the Results (right) tab.

1.5. Expert mode: additional functions

As already indicated the expert mode includes mainly the definition of time dependent parameters. The dose rate therefore becomes in general time dependent and the age value is thus the result of an iteration process as described in 2.2.3.

The use of the expert mode requires a more detailed knowledge of the investigated system and should be restricted to sophisticated questions. Nevertheless, it opens the opportunity to examine complex systems which cannot be investigated by the constant dose rate approach in a satisfying and sufficient way.

The *Expert mode* switch is located at the right side of the Menu / Icon bar. Please note that switching on this mode changes the file structure so that data loss may occur when switching off again. This risk is indicated by a warning message.

1.5.1. Data window

General data

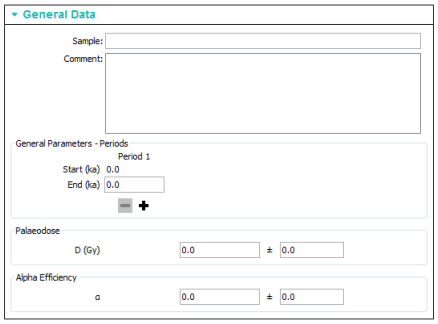

Figure 10 General data frame, as shown when opening a new project in the *Expert mode*.

In the *Expert mode* the history of the system can be divided into several *Periods*. The creation of these periods is added to the *General data* frame. Periods can be added or deleted by using the "+" and "-" buttons. For each period the *End* (older time boundary) must be defined. In Period 1, Start = 0 means the present; for all other periods the start is automatically set equal to the end of the next younger period. The correct chronological order of the end points is controlled by the software. A maximum number of 5 periods is definable.

For each period the following parameters can be set independently from other periods: the overburden properties in the *Cosmic radiation* frame, the *Moisture* in the *External dose* frame and the exchange parameters *Q* and *P* for open systems in radioactive disequilibria (see 2.3.4).

Note that during the calculation process age data older than the *End* data of the oldest period may occur. In this case all input data values from the oldest *End* are unvariedly extended up to the age to avoid an undefined software status. The user should take care for defining appropriate parameters in this "undefined" time interval [oldest *End* ... age].

Grain properties

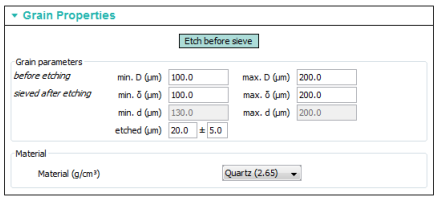

Figure 11 Example of an *Etch before sieve* process in the *Expert mode*.

Under some circumstances etched grains may be sieved again to restrict the range of grain size. This case of sieving after etching is treated in the *Expert mode* by clicking the *Etch before sieve* button in the *Grain properties* frame. Necessary inputs are then: the original grain diameter range *before etching* (*min. D* … *max. D*), the estimated *etched* layer thickness and the grain diameter range extracted by the final sieving (*sieved after etching*; *min.* δ ... *max.* δ). The result shown in the greyed frames is the diameter range (*min.* d … *max.* d) of the unetched grains which becomes available by this procedure.

An example is given in Figure 11. Taking into account the uncertainty of the etched layer the final 100 … 200 µm sieving extracts grains of a potential diameter range 130 … 250 µm in the unetched state. Since the diameter range was limited by the first sieving to 100 … 200 µm, only the 130 … 200 µm range of unetched grains is available for investigation.

Cosmic radiation

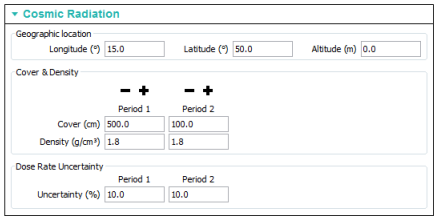

Figure 12 Example of a variable cosmic radiation in the *Expert mode*.

The overburden parameters can be varied from period to period in the *Cosmic radiation* frame. This includes the thickness of overlying material (*Cover*), its mean bulk *Density* and the dose rate *Uncertainty*. With that it is possible to simulate sedimentation / erosion processes affecting the cosmic dose rate. For the relevance of simulating variations in the cosmic dose rate see the discussion in chapters 2.1.2 and 2.3.1.

Internal dose

There are no additional functions in the *Expert mode* for the calculation of the internal dose rate.

External dose

The external dose rate is the most sensitive quantity for changes or special cases in the environmental conditions. To understand the meaning and the consequences of the input data in the following text it is strongly recommended to study the related chapters in the tutorial (2.3.2 to 2.3.4).

Moisture

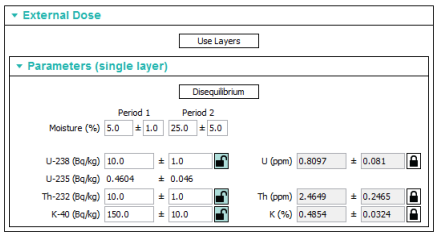

Figure 13 Example for different moisture levels in the periods.

For the significance of modeling *Moisture* variations from period to period due to changing climatic and / or hydrologic conditions see chapter 2.3.3. The input takes place in the upper part of the respective frame as shown in Figure 13.

Layer structure

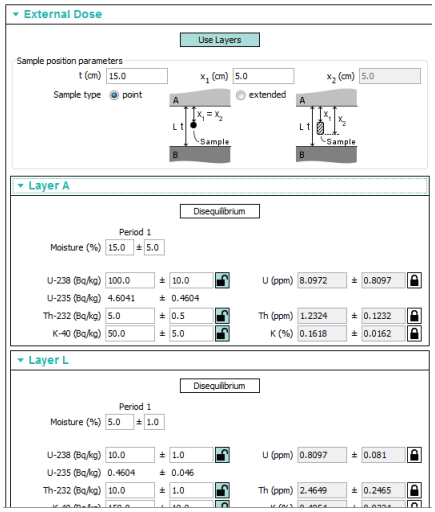

Figure 14 Appearance of the *External dose* frame in the case of layered geometries.

For the consideration of sandwich or layered structures as described in chapter 2.3.2 one has to switch on the button *Use Layers* in the *External dose* frame. The frame is now divided into three subframes as shown in Figure 14. The layered structure consists of an *Layer L* of limited thickness *t* enclosed by *Layer A* (above) and *Layer B* (below) of infinite extension. The sample material was taken either at one spot (*Sample type point*, sample extension negligible compared to thickness *t*) at depth x_1 or from an extended zone (*Sample type extended*) between depth x_1 and x_2. The sampling situation is illustrated by two sketches. Extended sample types may be applied e.g. for dating of potsherds which were found in an embedding sediment. *t* is then the original thickness of the sherd from which the region x_1 … x_2 was sampled.

Each of the layers A, B and L have identical structures of their input frames. Even in the case of radioactive disequilibria (see below) all layers can be designed independently.

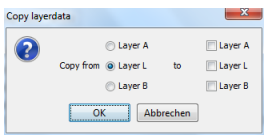

Figure 15 Window opened by the *Copy layer data* button.

If two layers are identical (one-sided dicontinuity or homogeneous cover of layer L) the data sets can be copied as needed from one layer to another by using the *Copy layer data* button (Figure 15).

Radioactive Disequilibria

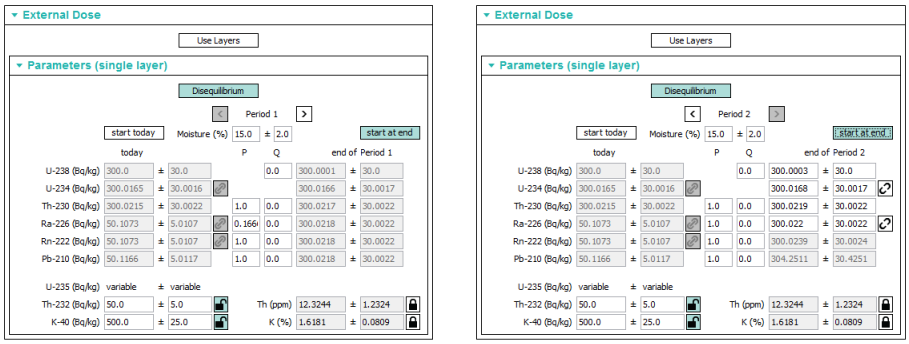

Figure 16 Example for data input in the case of radioactive disequilibria.

The treatment of radioactive disequilibria is enabled by pressing the *Disequilibrium* button. Disequilibria are considered for all longer living radionuclides of the ^{238}U decay series and the mobile noble gas Radon: ^{238}U, ^{234}U, ^{230}Th, ^{226}Ra, ^{222}Rn and ^{210}Pb. Short living daughters of these nuclides are assumed to be in equilibrium with the parent (example: ^{214}Pb and ^{214}Bi are in equilibrium with ^{222}Rn) The only allowed input quantities are specific activities; in contrast to the equilibrium mode the entry of contents is disabled. Disequilibria in the ^{232}Th decay series are not treated because of their short lifetime in this chain. Also ^{235}U disequilibria are neglected because of their low contribution to the radiation field. The input of the specific activity or concentration of ^{232}Th and ^{40}K is the same as in the equilibrium case. The activity function of ^{235}U is set to be parallel to ^{238}U according to the natural ^{235}U / ^{238}U activity ratio.

The time evolution of a disequilibrium can be developed from two starting points - either from the current situation or from the moment of deposition of the dated material. The user may switch between these two options by the *start today* / *start at end* buttons. Especially for open systems a start at deposition is the preferable choice.

If at the starting point a nuclide is in equilibrium with its successors, this condition is enforced by clicking the button next to the input frame of the nuclide.

One can switch between the different periods by clicking on the arrows besides the *Period i* label. Thereby the calculated modern activities (below the *start today* button) are permanently displayed for controlling the agreement with the present analytical results. The right block of activity data refers to the older boundary of the displayed period. *P* and *Q* are exchange parameters for open systems (cf. chapter 2.3.4) and valid for the shown period. For mathematical reasons *P* cannot be defined for ^{238}U. The *Q* value of ^{234}U is set to be identical with that of ^{238}U. It is advisable to minimise the number of *P*, *Q* values deviating from the default values 1 and 0, respectively. The results may contain no physical sense although any input is allowed. As a control the activity time functions shown in the Results / Report window should be checked to be reasonable.

The example in Figure 16 comprises a start of the time evolution at deposition, where the decay series showed a radioactive equilibrium. The equilibrium is not affected in *Period 2* whereas in the younger *Period 1* five sixths of the newly formed ^{226}Ra are removed from the (open) system. ^{226}Ra is assumed to be at any time in equilibrium with its successors ^{222}Rn and ^{210}Pb. In Figure 16 the display status of the *External dose* frame is shown for both defined periods.

1.5.2. Results / Report window

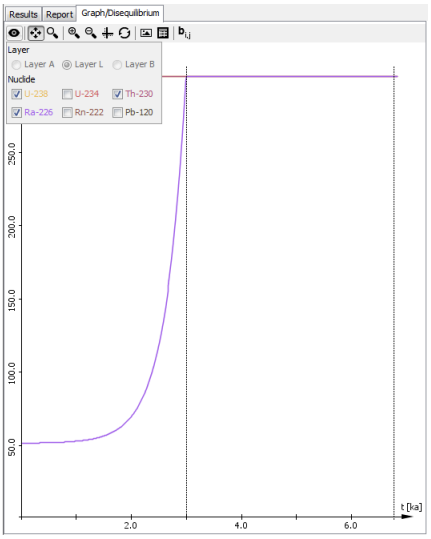

Figure 17 Example for a graph of the disequilibrium time evolution. The pressed button allows the selection of individual radionuclides.

In the *Expert mode* a *Graph / Disequilibrium* tab is added to the window. It contains a graphical presentation of the time dependent activities of the considered members of the ^{238}U decay series. The plot example in Figure 17 is based on the data used in Figure 16.

The menu bar in the upper part of the *Graph / Disequilibrium* window has the following items:

Button opens a window for general display properties. This includes the selection of the displayed radionuclides and - in the case of a layered structure - the selection of the layer for which the disequilibrium has to be shown.

Indicator that the cutout selected by the subsequently described buttons can be moved over the graph.

Definition of a region to be zoomed in.

Zoom in / zoom out

Definition of a region to be zoomed in by input of the age and activity range.

Reset of the zoom regions to the full display.

Saves the displayed graph as an image file (*.png).

Saves the displayed data in tabular form. Age range, increment and radionuclides can be selected by pressing the *Options* button.

Output of the matrix elements b_{ij} used for the mathematical formulation of the disequilibrium (see 2.3.4)

The *Report* frame differs from that in the *Standard mode* only by the addition of the period definitions.

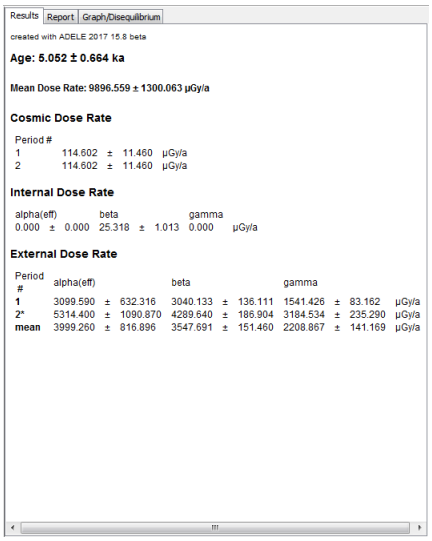

Figure 18 Example of a *Results* tab in the *Expert mode*.

In the *Results* frame values of the cosmic and the external dose rate components are presented separately for each period (Figure 18). These data must be understood as mean values averaged over each period length because of the potential time dependence of all dose rate components. Additionally, for the external dose rate a “mean” value is given for each component meaning the average over the total calculated age.

1.6. Examples of dating radioactive disequilibria

As indicated in chapter 1.5.1 the dating of systems showing radioactive disequilibria may become a complicated task. For this reason the application of **ADELEv2017** to two characteristic cases is illustrated in the following.

Because of the identity of the moment of deposition (= age value) with the start of the activity evolution an iterative procedure must be applied. This process must be performed "manually" since at the present state an automated iteration is not implemented in the software yet.

The model system is a fictional one, so arbitrary but not senseless parameters were selected for the description of the computational procedure. As investigated material the polymineralic fine grain fraction was chosen. A palaeodose of **D = (50 ± 5) Gy** was determined by OSL.

Cosmic radiation	
Longitude	13.5° E
Latitude	51° N
Altitude	400 m
Cover	100 cm
Cover density	1,8 g cm^{-3}

Grain properties				
Grain size [µm]	**Material**	**Density [g cm^{-3}]**	**Etched layer [µm]**	**a-value**
7 - 10	Feldspar	2.55	-	0.10 ± 0.02

Internal dose parameters		
U [ppm]	**Th [ppm]**	**K [%]**
0	0	12.5 ± 0.5

External dose parameters				
Specific activity [Bq kg^{-1}]				**Moisture [%]**
^{238}U series		**^{232}Th series**	**^{40}K**	**current**
^{238}U	^{226}Ra			
300 ± 30	50 ± 5	50 ± 5	500 ± 25	**15 ± 2**

Table 1 Input parameter for **ADELEv2017** of the investigated model system.

All other parameters necessary as the input for **ADELEv2017** are listed in Table 1. The surrounding material shows a clear radioactive disequilibrium between ^{238}U and ^{226}Ra. Two assumptions about the nature of the system were tested:

Thesis I: The system is closed. Two initial equilibria were present at the moment of deposition: one equilibrium from ^{238}U to ^{234}U and a second one including ^{230}Th and its followers. Such a model system with an initial ^{234}U / ^{230}Th disequilibrium can be found e.g. in

organic sediments sealed by clayey layers (as used for U / Th dating). The equilibrium of the whole ^{238}U decay series is restored on a timescale given by the half life of ^{230}Th of 75,000 a.

Thesis II: The system is open with a constant Uranium uptake during the whole time since deposition. At the moment of sedimentation the ^{238}U decay series was in equilibrium. An example of such a system is a water-bearing mixture of a mineralic detritus with admixed calcareous shells.

To start the calculation procedue, a rough age estimate is necessary. Here we assume that the sediment was deposited maximum 10 000 a before present.

Procedure for age calculation applying thesis I:

- start with the input of all parameters and set the end of period 1 to 10 ka
- in the *External Dose* frame press the *Disequilibrium* button, press *start today*, set U-238 to (300 ± 30) Bq kg^{-1} and force the equilibrium of the total series (🔗) (Figure 19, left)
- go to *start at end* and allow the equilibrium from ^{230}Th on (Figure 19, middle)
- change the ^{230}Th activity until the present ^{226}Ra activity is about the desired 50 Bq kg^{-1} (Figure 19, right). Here we continue with ^{230}Th = 37 Bq kg^{-1}.

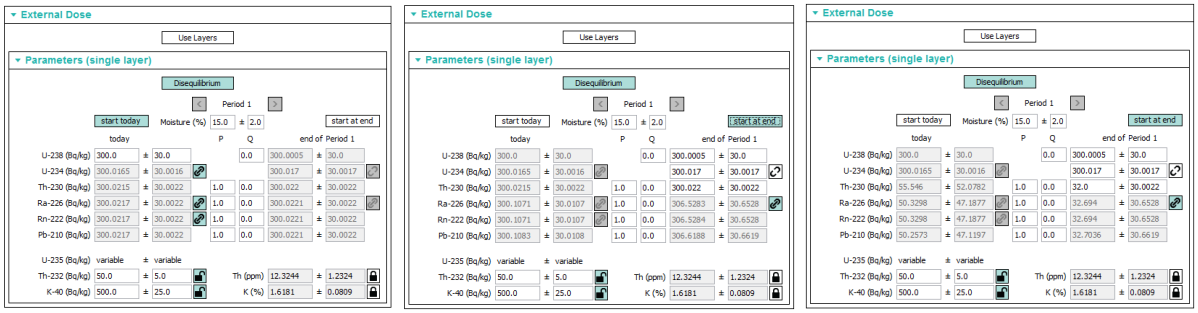

Figure 19 First steps of the calculation procedure applying thesis I.

- the first age estimate, shown in the *Results* frame, is now 7.718 ka. Since the age must be identical with the start of the activity evolution, change now the end of period 1 to 7.718 ka.
- vary again the ^{230}Th activity value until the present ^{226}Ra activity becomes 50 Bq kg^{-1}.
- take the new age estimate from the *Results* frame and use it as end of period 1.
- reiterate the last two steps until the age from the *Results* frame coincides with the end of period 1.
- chose the uncertainty of the ^{230}Th activity so that the present ^{226}Ra activity gets the right uncertainty. The final *External Dose* frame is shown in Figure 20.

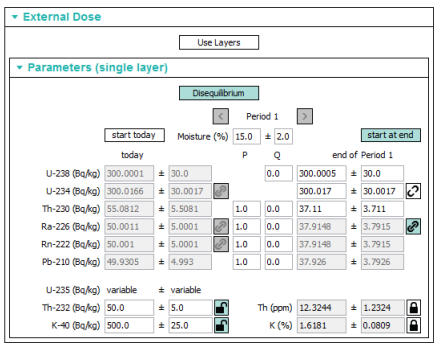

Figure 20 *External Dose* frame at the end of the calculation.

The age result of this procedure is (7.70 ± 0.96) ka. Figure 21 shows the activity functions for ^{238}U, ^{230}Th and ^{226}Ra in this case, i.e. when thesis I is assumed.

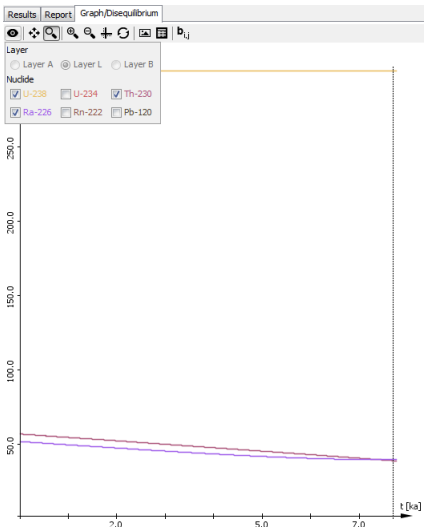

Figure 21 Activity development when applying thesis I.

Procedure for age calculation applying thesis II:

- start with the input of all parameters and set the end of period 1 to 10 ka
- in the *External Dose* frame press the *Disequilibrium* button, press *start at end* and set the ^{238}U decay series in equilibrium (🔗) with a starting value of 50 Bq kg^{-1}. (Figure 22Figure 19, left)
- change the uptake parameter Q for ^{238,234}U until the present ^{238}U activity is about the desired 300 Bq kg^{-1} (Figure 22Figure 19, middle). Here we continue with Q = 0.025.
- the first age estimate, shown in the *Results* frame, is now 8.486 ka. Since the age must be identical with the start of the activity evolution, change now the end of period 1 to 8.486 ka.
- vary the Q value **and** the ^{238}U activity until the present ^{238}U and ^{226}Ra activities becomes 300 Bq kg^{-1} and 50 Bq kg^{-1}, respectively. (Figure 22, right)
- take the new age estimate from the *Results* frame and use it as end of period 1.

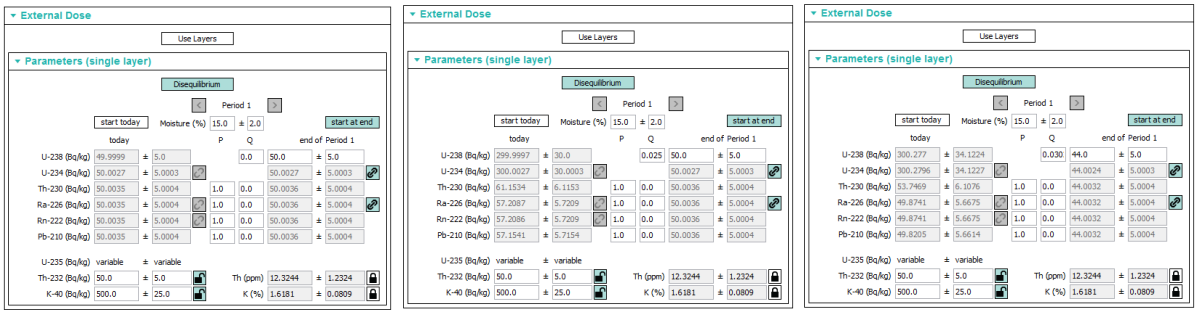

Figure 22 First steps of the calculation procedure applying thesis II.

- reiterate the last two steps until the age from the *Results* frame coincides with the end of period 1.
- chose the uncertainty of the ^{238}U activity so that the present ^{238}U activity gets the right uncertainty. The final *External Dose* frame is shown in Figure 23.

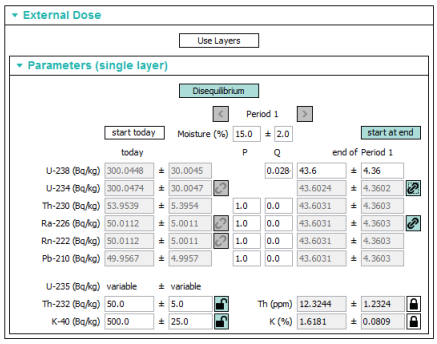

Figure 23 *External Dose* frame at the end of the calculation.

The age result of this procedure is (9.0 ± 1.1) ka at a starting value of 43.6 Bq kg^{-1} for the ^{238}U decay series and an ^{238,234}U uptake parameter of 0.02842 Bq kg^{-1} a^{-1}. Figure 24 shows the activity functions for ^{238}U, ^{230}Th and ^{226}Ra in this case, i.e. when thesis II is assumed.

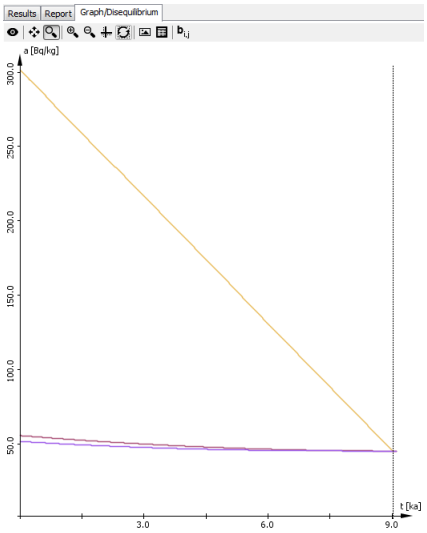

Figure 24 Activity development when applying thesis II.

2. Tutorial

2.1. The radiation field in natural environment

The basis of luminescence and ESR dating as dosimetric methods is the omnipresence of a radiation field in the environment which results in the deposition of radiation energy in solids. Two major phenomena have to be considered to understand this energy transfer to matter: the occurrence of long living radionuclides in the Lithosphere and the permanent succession of nuclear reactions in the stars. These phenomena are linked with the terms *natural radioactivity* and *cosmic radiation*.

2.1.1. Natural radioactivity

A short introduction into radioactivity

Radioactivity denotes the ability of atomic nuclei to change their composition. The probability that a nucleus suffers a transformation within a certain time interval is constant for its lifetime. Thus, the probability that one of N nuclei decays within this interval and therefore the actual rate of transformations is proportional to N:

$$\frac{dN}{dt} = -\lambda N \qquad \text{(Eq. 1)}$$

where

N - number of nuclei
t - time

The negative sign is used since the number of nuclei decreases with time.

The solution of the differential equation in Eq. 1 is

$$N = N_0 \cdot e^{-\lambda t} \qquad \text{(Eq. 2)}$$

N_0 - initial number of nuclei at t = 0

The factor λ is called the *decay constant*. The term *half life* ($T_{1/2}$) describes that time interval after which N(t) is only one half of the initial value N_0; it is related to λ according to

$$\lambda = \frac{\ln(2)}{T_{1/2}} \qquad \text{(Eq. 3)}$$

The run of the curve deduced from Eq. 2 and 3 is shown in Figure 25. After 1, 2, 3, ... half lives the number of nuclei is $\frac{1}{2^1}$, $\frac{1}{2^2}$, $\frac{1}{2^3}$ ... of the initial value N_0.

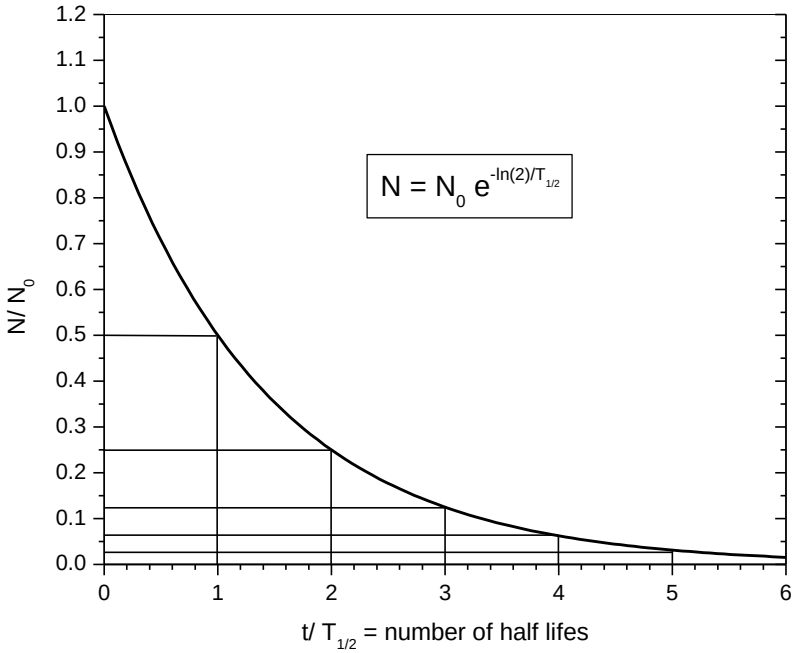

Figure 25 Ratio of the number of nuclei N to its initial value N_0 as a function of the number of the elapsed half lifes in a radioactive decay.

The *activity* A denotes the decay rate and has the unit Becquerel Bq (1 Bq = 1 decay per second). It shows the same time dependence as N:

$$A(t) = \left|\frac{dN(t)}{dt}\right| = \lambda \cdot N = \lambda \cdot N_0 \cdot e^{-\lambda t} \qquad \text{(Eq. 4)}$$

with $A_0 = \lambda \cdot N_0$ as start value.

Looking at the physical background of radioactivity, one must consider the composition of the atomic nucleus. In a simple model an atomic nucleus consists of Z protons and N neutrons. A certain type of nuclei, as described by Z and the mass number A = Z + N is called *nuclide* and written by the formula ${}^{A}_{Z}X$. Note that the term isotope describes nuclides with the same Z. The two denotations should not be confused.

A nuclear "decay" is hence a transformation of one nucleus into another of different composition. Spontaneous transitions between two states are necessarily connected with an energy loss of the initial nucleus. This is depicted by the usual presentation form of decay schemes. The example in Figure 26 shows the β^- decay of ^{210}Pb from the uranium decay series combined with the emission of a 46.5 keV gamma quant.

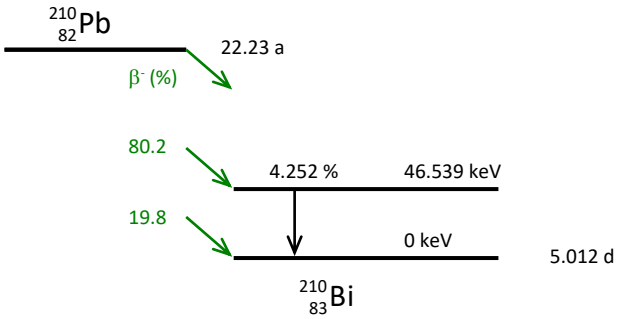

Figure 26 Decay scheme of ^{210}Pb. ^{210}Pb decays to the ground state of ^{210}Bi in two ways: (i) β^- decay + emission of a γ-quantum of 46.539 keV (80.2 % probability), (ii) β^- decay alone (19.8 %). (Data from [3])

Different modes of nuclear transformations are known, the most common are called *alpha-* and *beta-decay*. In this chapter we describe the interaction of the emitted radiation with matter as general as is necessary to understand the dosimetric consequences; more detailed descriptions can be found in literature.

Decay types and radiation characteristics

Alpha decay is the release of a helium nucleus (${}^4_2\mathrm{He}$) from the initial nucleus ${}^A_Z\mathrm{X}$ and is written as

$$ {}^A_Z\mathrm{X} \rightarrow {}^{A-4}_{Z-2}\mathrm{Y} + {}^4_2\mathrm{He} \qquad \text{(Eq. 5)} $$

The kinetic energy of the α-particles is well defined and commonly in the range of 4 ... 9 MeV. Due to the conservation of momentum the daughter nucleus receives a recoil energy in an order of magnitude of 100 keV. The α-particle itself decelerates by collisions with atoms whereby the highest energy loss occurs at the end of its path ("Bragg-peak", cf. Figure 27). Typical α-ranges in matter amount to some 10 µm thus leading to densities of the released energy of some 10^{15} eV / cm³. The high concentration of energy compared to other types of decay (see below) has important effect on the luminescence stimulation (see chapter 2.2.3).

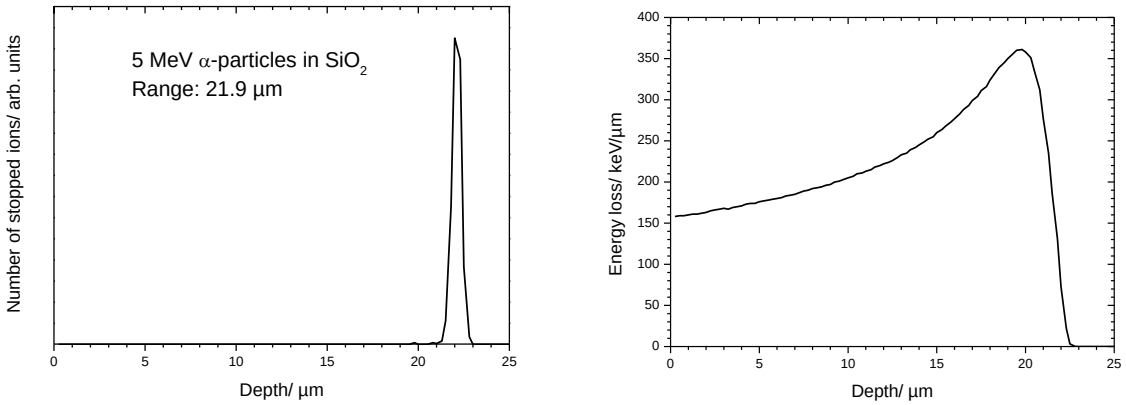

Figure 27 Longitudinal distribution of stopped particles (*left*) and energy loss per path length (*right*) for 5 MeV α-particles entering pure SiO_2 (Calculated with SRIM code [4])

Beta decay can be described as a conversion of a neutron n into a proton p (β^- decay) or vice versa (β^+ decay). For the sake of charge conservation an electron (e^-) or positron (e^+) is emitted in this process. Additionally an electron antineutrino $\bar{\nu}_e$ or electron neutrino ν_e, respectively, is released:

$$ {}^{1}_{0}n \rightarrow {}^{1}_{1}p + {}^{0}_{-1}e^{-} + \bar{\nu}_e \qquad \text{(Eq. 6)} $$

$$ {}^{1}_{1}p \rightarrow {}^{1}_{0}n + {}^{0}_{1}e^{+} + \nu_e \qquad \text{(Eq. 7)} $$

As a consequence of the conservation of energy and momentum the emitted e^- or e^+ shows a continuous energy spectrum ranging from 0 keV to a maximum called the end-point energy (15 keV to 3.3 MeV for natural radionuclides). The anti-particle e^+ has a lifetime in solids of some 10^{-10} s and annihilates at its first collision with an electron under the emission of two 511 keV photons.

For electrons the energy loss when penetrating a material is described by the stopping power S(E):

$$ S(E) = \frac{dE}{dx} \cdot \frac{1}{\rho} \qquad \text{(Eq. 8)} $$

E - electron energy,
x - path length,
ρ - density of the penetrated material.

S(E) is strongly energy dependent and decreases in the considered energy range whereas the maximum path length, the range, varies up to values of some mm for 1 MeV electrons in pure SiO_2 (Figure 28).

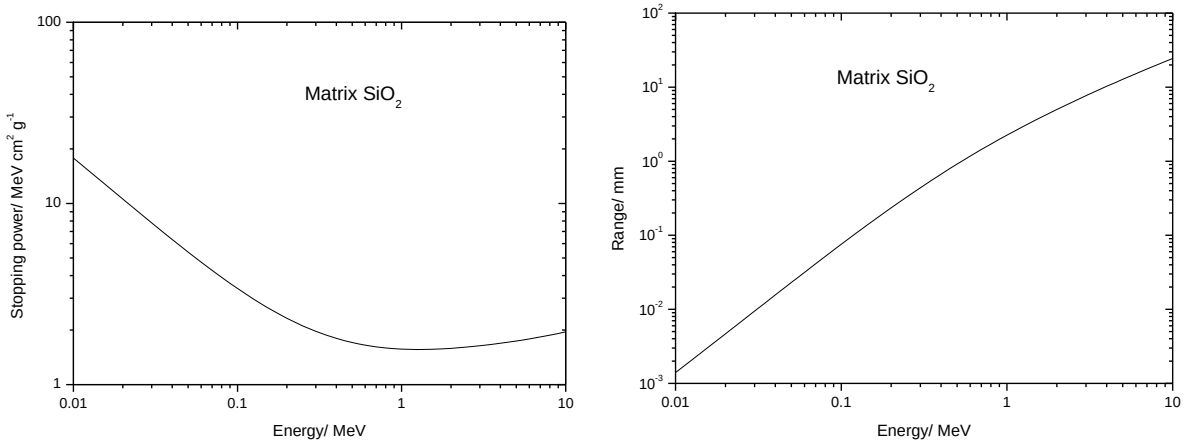

Figure 28 Stopping power (*left*) and ranges (*right*) for electrons entering pure SiO_2 [5]

Because of the gas filled space between grains electron or β^- particle ranges in sediments are somewhat longer but do not exceed some mm.

Gamma radiation is emitted if a nucleus undergoes a deexcitation from a higher energy level to a lower one or to the ground state. Unlike α or β decay it does not cause a change in the proton or neutron number. By its nature, this radiation is electromagnetic and can be described either as a wave or as a photon. Energy level difference ΔE and frequency f of the emitted photon are connected by Planck's constant h:

$$\Delta E = h \cdot f \qquad \text{(Eq. 9)}$$

Naturally occurring radionuclides emit gamma rays in the energy range from 40 keV to 3 MeV. Alpha and beta decays are often followed by gamma emissions whereas only a few nuclides are pure gamma emitters i.e. they occupy a long living metastable level above the ground state.

A collimated beam of gamma rays with intensity I_0 will be attenuated by a material layer of thickness d according to the absorption law:

$$I(d) = I_0 \cdot e^{-\mu d} \qquad \text{(Eq. 10)}$$

I(d) - intensity at thickness d
μ - attenuation coefficient

Since the term “range” does not really makes sense for gamma quanta, the half value layer (HVL) is used instead as a typical parameter. It is a function of the photon energy and describes the thickness of a certain material that is necessary to reduce the intensity of the incident radiation to 50 %. For example, a thickness of three HVL is equivalent to a reduction to 12.5 % of the initial intensity. Exemplary HVL for a gamma energy of 1 MeV are 4.7 cm for pure SiO_2 and 6.3 cm for a mixture of 70 % SiO_2 and 30 mass-% H_2O (as a soil-like composition).

Treating γ ray attenuation by equation (10) is not the full truth: this relation describes only the behaviour of photons without any interaction with matter but not the dose rate decrease! Inelastically scattered γ quanta from each point of the system will also contribute to the local energy deposition and therefore the dose decrease will be much slower. Nevertheless, equation (10) gives an idea about the scale at which γ radiation interacts with the matrix.

Compared to α and β particles gamma rays penetrate further in matter but on the other hand they deposit the lowest energy density in the material.

Figure 29 summarises on a logarithmic scale at which radii around a radiation source the matrix is affected by interactions of the three types of ionising radiation. The penetration depth of the cosmic radiation component is also shown (cf. chapter 2.1.2).

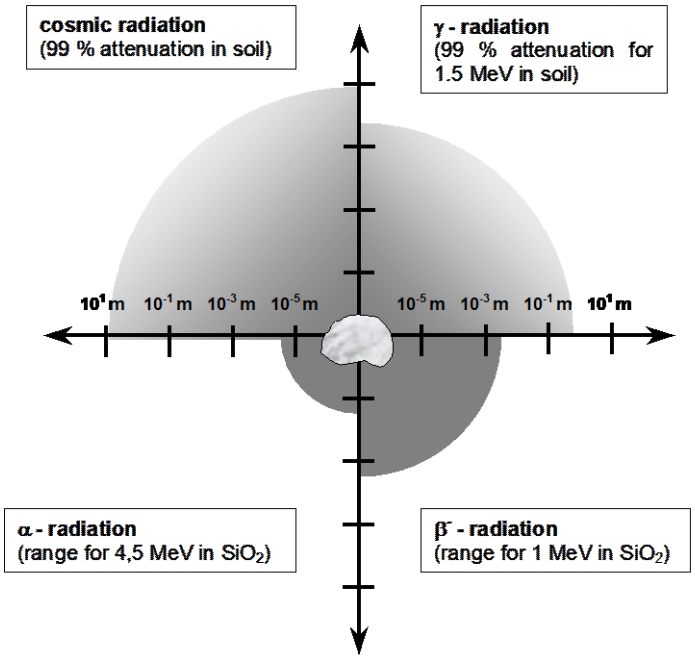

Figure 29 Radii of impact for the different radiation types relevant in dosimetric dating.

The amount of ionising radiation energy absorbed per mass of the material is the definition of the term *dose* or *energy dose*. The unit for the dose D is called the Gray Gy (1 Gy = 1 J kg^{-1}). Note that in luminescence dating "equivalence dose" is often used for the quantity determined by the evaluation of the luminescence measurements. It should not be mixed up with "equivalent dose" which is a measure of the effect of radiation on biological matrices. For this reason, the use of the term "palaeodose" is less misleading and will be used in the **ADELEv2017** software.

The term "dose rate", often written as $\dot{D}$, is used for the energy dose absorbed per time. Common units of dose rates in luminescence dating are mGy a^{-1} and Gy ka^{-1}.

Natural radioactivity in the environment

The synthesis of the elements during the history of the universe (about 10^{10} a) did not only produce stable elements but also a number of radioactive nuclides. Those with half lifes > 10^9 a can still be detected in the environment and are called *primordial* nuclides. The most important ones because of their contribution to the natural radiation field are ^{238}U, ^{235}U, ^{232}Th, ^{40}K and ^{87}Rb where the first three of them do not directly decay to stable nuclides. They are the starting points of decay series passing through daughter isotopes of various elements and with half lifes ranging from 10^{-4} s to 10^5 a until they reach the stable lead isotopes ^{206}Pb, ^{207}Pb and ^{208}Pb, respectively. These decay series as well as ^{40}K and ^{87}Rb are presented in Figure 30, Figure 31 and Figure 32 together with the decay types and the half lives. Dark green boxes mark nuclides with gamma emission probabilities > 1 %, light green means that the maximum gamma emission probability is < 1 %.

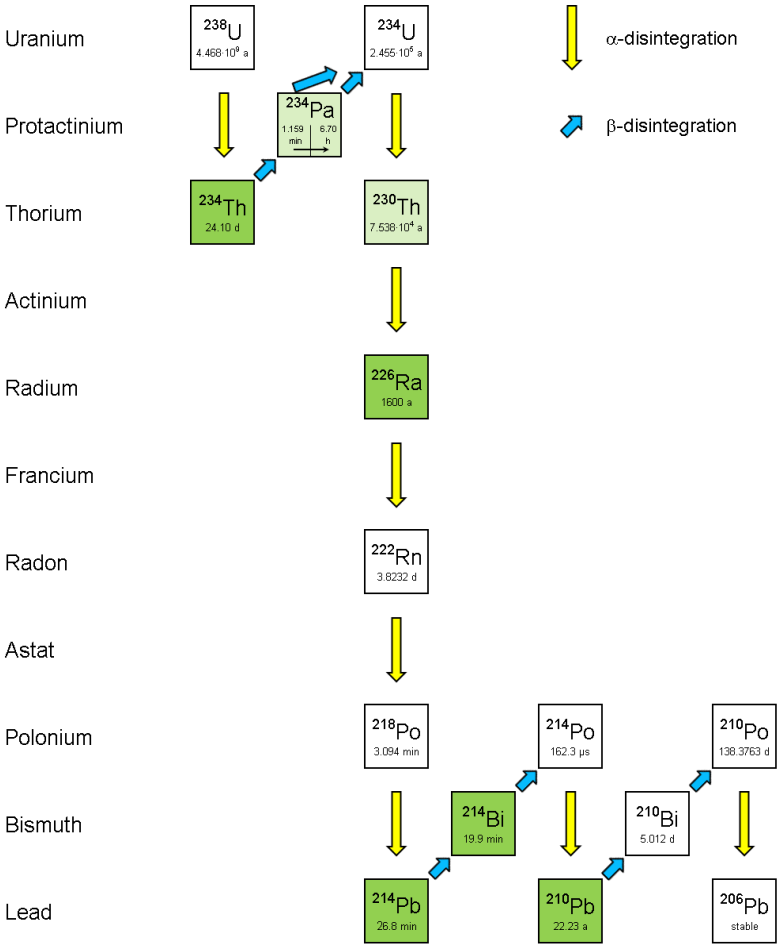
Uranium
Protactinium
Thorium
Actinium
Radium
Francium
Radon
Astat
Polonium
Bismuth
Lead
238U 4.468·10^9 a
234U 2.455·10^5 a
234Pa 1.159 min 6.70 h
234Th 24.10 d
230Th 7.538·10^4 a
226Ra 1600 a
222Rn 3.8232 d
218Po 3.094 min
214Po 162.3 µs
210Po 138.3763 d
214Bi 19.9 min
210Bi 5.012 d
214Pb 26.8 min
210Pb 22.23 a
206Pb stable
α-disintegration
β-disintegration

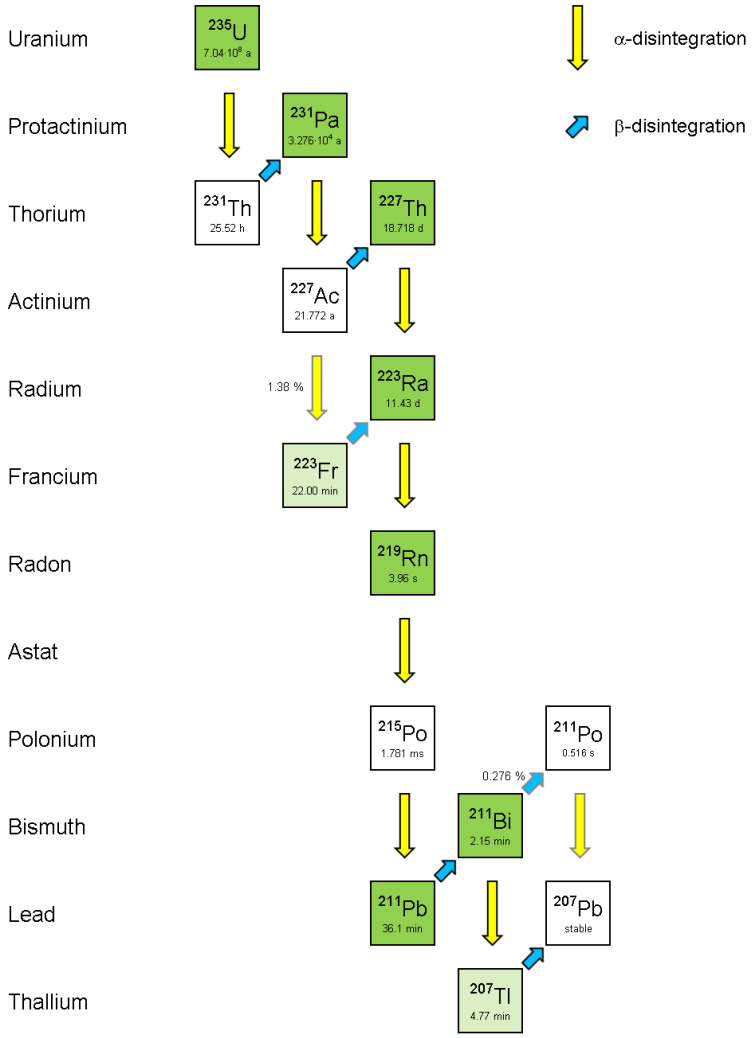

Figure 30 Natural decay series of ^{238}U (above) and ^{235}U (below) along with the most important decay properties of the included radioisotopes (half life and prevailing decay type) [3].

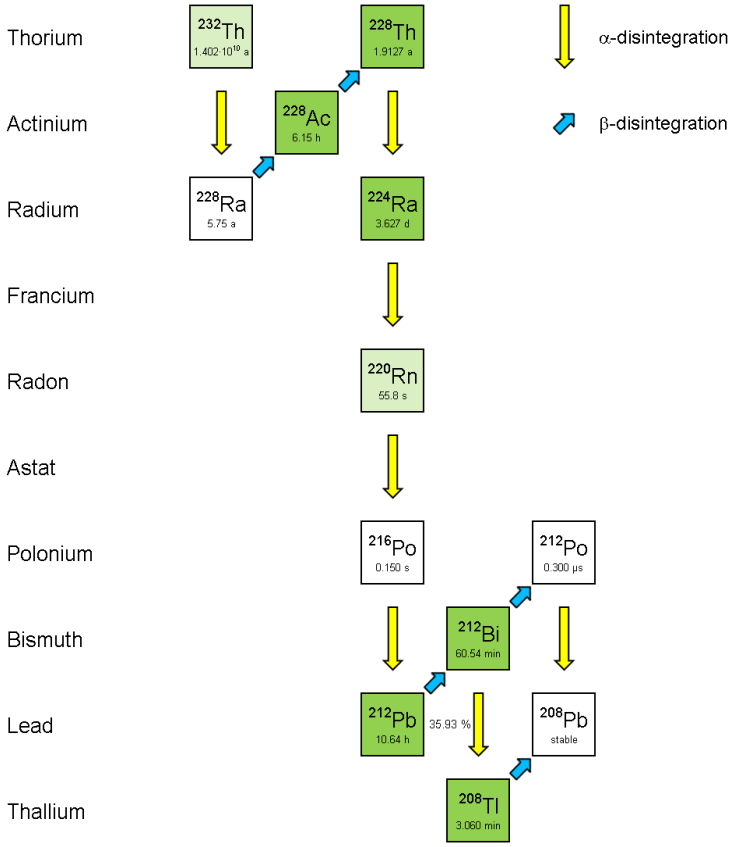

Figure 31 Natural decay series of ^{232}Th along with the most important decay properties of the included radioisotopes (half life and prevailing decay type) [3].

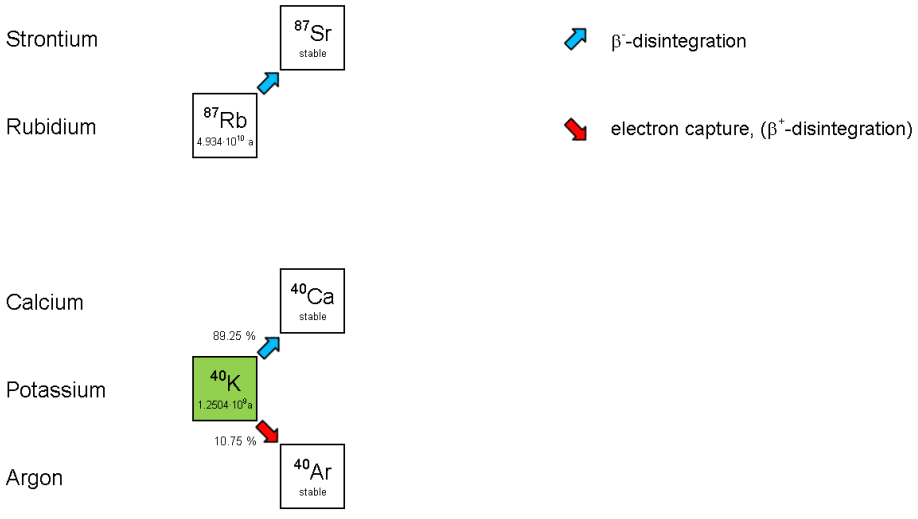

Figure 32 Decay of ^{87}Rb (above) and ^{40}K (below) along with the most important decay properties of the included radioisotopes (half life and prevailing decay type) [3].

The importance of this set of radionuclides results from their omnipresence in the lithosphere: the mean element concentrations in the upper continental crust are 2.5 ppm for

U (equivalent to a specific activity of 31 Bq ^{238}U per kg crust material), 10.3 ppm for Th (42 Bq ^{232}Th per kg), 2.87 % for K (887 Bq ^{40}K per kg) and 110 ppm for Rb (96 Bq ^{87}Rb per kg) [6].

Element	Mean concentration in earth crust	Radionuclide(s)	Dose rate [mGy a^{-1}]		
			alpha	beta	gamma
U	2.5 ppm	^{238}U decay series	6,69	0,35	0,27
		^{235}U decay series	0,30	0,01	0,01
Th	10.3 ppm	^{232}Th decay series	7,60	0,29	0,49
K	2.87 %	^{40}K		2,29	0,71
Rb	110 ppm	^{87}Rb		0,04	

Table 2 Dose rate contributions in a homogeneous sediment containing the mean crust concentrations of radioactive elements (calculated with the conversion factors from [7]).

As shown in Table 2, the main contributions to the dose rate in a sediment come from the decay series of ^{238}U and ^{232}Th as well as from ^{40}K. The decay chain of ^{235}U and the isotope ^{87}Rb provide only minor contributions which are in the order of the uncertainty of the other components.

Whereas ^{40}K and ^{87}Rb behave geochemically as potassium and rubidium, the chemical and physical properties of members of the decay series are different from that of uranium and thorium. This fact may lead to differentiation processes which are treated more comprehensively in chapter 2.3.4. In an undisturbed geological situation all nuclides of the decay series tend to a stationary state at which formation and decay rate are equal for each member. This state characterised by an uniform activity along each series is called *radioactive equilibrium*.

2.1.2. The cosmic ray component

The primary cosmic radiation flux consists of about 90% protons, 9 % alpha particles and about 1 % electrons or heavier particles [8]. Collisions of cosmic ray particles with molecules (mainly N_2, O_2) in the earth' atmosphere lead to the production of a complex cascade of secondary particles. Downwards to the earth surface the composition of these secondaries changes. At sea level up to mid altitudes it is just the muon, neutron and electron component which plays a significant role in producing a *cosmic ray dose* rate relevant for luminescence dating. As the latter (together with a much smaller photon component historically termed as "weak" or "soft" component) is attenuated by a few 10 cm of soil there remains just a "hard" component (muons) and the nucleonic component (mainly neutrons). The neutron induced dose rate is rapidly attenuated with a mean length of about 200 g cm^{-2} (corresponding to about 1 m of sediment) [8]. In deeper layers, the muonic component plays the most important role in dose deposition derived from cosmic particle flux.

There is a variation of the cosmic radiation on the earth's surface induced by the magnetic field. Charged cosmic particles reach more easily the top of the atmosphere at the poles by

travelling down around the field lines [9]. As a result there is a slight increase of the cosmic dose rate at the surface from the equator to a “knee” in the latitude effect at about 40°.

However, the most effective parameters influencing the cosmic dose rate at the position of a sampled sediment are the shielding by air and by sediment overburden or other rock or water shieldings. Therefore the vertical position in the lithosphere at which the dating object was stored (i.e. altitude, material type and thickness of overburden as well as duration of shielding) is important for calculating a reliable cosmic dose in luminescence dating.

Robust tools for calculation of the cosmic dose rate in dependence of geographical latitude, longitude and altitude as well as of the burial depth and cover material are given in the papers of Prescott and Hutton [10], [11]. The formulae presented there require the knowledge of the total mass per area (i.e. the area density) above the sampling position. This means that at the one hand the density of the coverage must be estimated and otherwise that layers of differing composition (e.g. water and sediment) can simply be considered by summing up their area densities.

It should be noted that the frequently used formula from [11] is valid only for the muonic component. The dose rate at shallow depths influenced by the soft and nucleonic component must be extracted from a plot shown in [10] (thanks to C.Burow for this hint!). A common systematic error of the cosmic dose rate component of ± 10 % must be taken into account due to primary cosmic ray fluctuations for all latitudes in the past 500 ka (± 30% if older [11]).

It is often argued that the cosmic dose rate (and hence uncertainties in its determination) is less important as it is small compared to that arising from the radioisotope content. This is however a very relative argument.

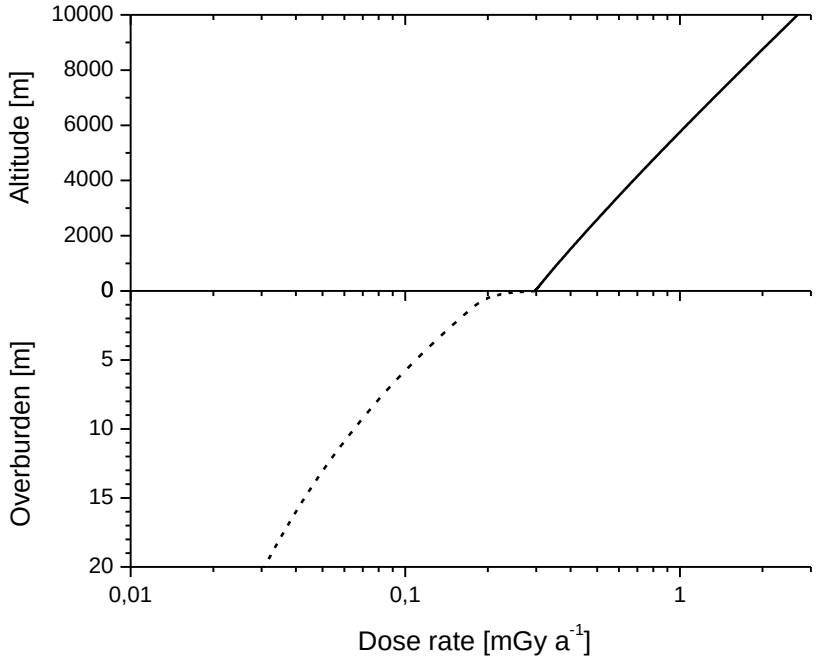

Figure 33 Dependence of the dose rate produced by interactions of cosmic rays. Above: at soil surface in various altitudes; below: at sea level with varying overburden (assuming a soil density of 2 g cm^{-3}).

The upper plot in Figure 33 gives the cosmic dose rate at soil surface as a function of altitude. In mountain areas this quantity may reach values in the order of 1 mGy a^{-1}. Thus for near surface sediments containing low radioactivity (quartz sands, carbonates etc.) the cosmic dose can amount for some 10 per cent of the total dose rate and is therefore no more of minor interest.

The sharp decrease of the cosmic dose rate in the uppermost soil layers reflects the shielding of the weak and the nucleus component. Below, this dose rate is determined by the reduction of the muon intensity at increasing coverage.

Particularly in the case of close to surface deposition the variation of the overburden has not to be neglected. Such variations may be caused by sedimentation or erosion processes as well as by fluctuating water levels. Such sampling positions should be avoided if possible. If samples must be taken near the surface the historical development of the cover layer has to be estimated for reliable assessments of the cosmic dose rate. One should be aware that such positions cause further problems in dose rate calculations like a reduced one-sided gamma radiation field and radioactive disequilibria like Radon loss or ^{210}Pb excess. It is recommended to test several bracketing situations for an evaluation of the enhanced age uncertainty produced by these imponderabilities. In **ADELEv2017** the user is able to define several time periods differing from each other inter alia by the mean density and the thickness of the covering material.

2.2. *Calculation of the dose absorbed by the dosimeter since the last zeroing - "Dose rate determination"*

After determining the dose accumulated since the last zeroing of the luminescence signal, i.e. the palaeodose, one has to calculate how long it took to collect this palaeodose. The result is then the exposition- or luminescence- age. This calculation requires a detailed analysis of the radiation sources in the sediment or sample and also some knowledge about the investigated grain fraction and about its treatment during sample preparation. The procedure is totally independent from the investigation of the luminescence signal (i.e. the determination of the palaeodose) and is based upon the basic principles of dosimetry.

2.2.1. The beginning: an ideal system

The general dosimetric approach in luminescence dating starts with considering an isotropic system of infinite size which contains a homogeneous radionuclide distribution. For the reason of uniformity, the system must be free of singularities i.e. a certain volume element emits and absorbs equal amounts of energy per time. This is the state of *radiative equilibrium* (not to be confused with the term *radioactive equilibrium*, cf. Chapter 2.1.1). The absorbed dose rate in the matrix can be calculated from the energy released per decay and from the radionuclide concentration. The ratio of dose rate (in Gy kg^{-1}) to specific activity (in Bq kg^{-1}) for a certain nuclide is called *conversion factor*, these values are tabulated in the literature (e.g. [7]). From these data the dose rate in the ideal infinite system $\dot{D}_\infty$ can easily be deduced for each radiation type (α, β and γ).

The contributions of the different decay types to the total dose rate $\dot{D}_\infty$ vary strongly between ^{40}K, ^{87}Rb and the members of the U and Th decay series as already mentioned in Table 2 for a system containing the mean radionuclide content of the earth crust.

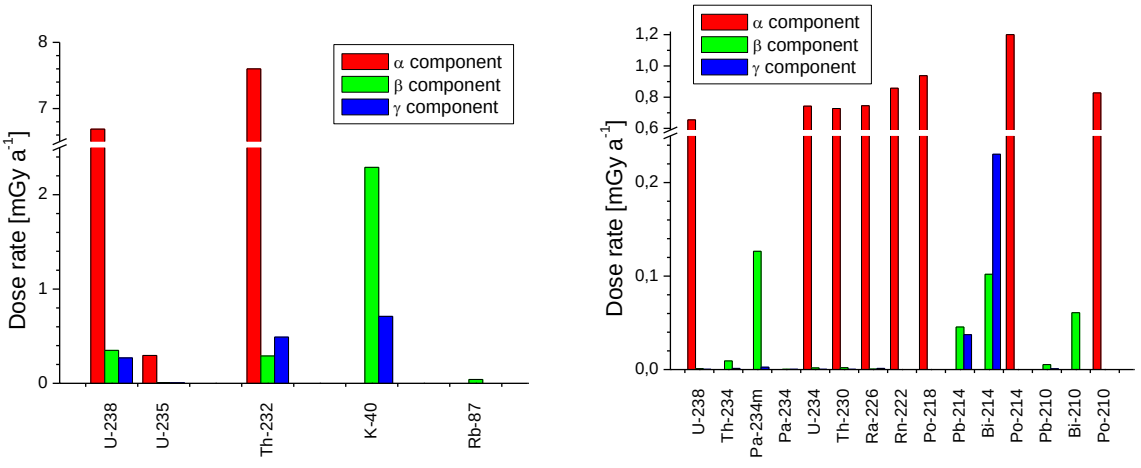

Figure 34 Contribution of different radiation components to the dose rate in an infinite ideal system containing the mean radionuclide content of the earth crust (cf. Table 2). Left: Total dose rates of the various decay series, ^{40}K and ^{87}Rb; Right: Distribution of different dose components within the ^{238}U decay series.

This fact is illustrated in the left plot of Figure 34. For the ^{238}U and ^{232}Th decay chain the α component is the dominant one and about one order of magnitude larger than those of the β- and γ-radiation. Being the component with the shortest range it is therefore most sensitive to heterogeneities of the nuclide contents.

^{40}K provides the major contribution to the β-component whereas the γ-dose rate is about evenly distributed between ^{238}U and ^{232}Th decay series and ^{40}K. The dose rates of the ^{235}U chain and ^{87}Rb are of minor importance or negligible, respectively. ^{87}Rb is therefore often neglected in dose rate calculations and will not be considered further in this chapter.

In the right picture of Figure 34 one finds the dose rate contributions of the members of the ^{238}U decay series to the total dose rate. It should be mentioned that the dose rate components are not uniformly distributed over the whole decay series. Within the decay series, the (β + γ) component originates to 77 % from nuclides "beyond" ^{222}Rn. This relation has consequences in the case of radioactive disequilibria, as will discussed in chapter 2.3.4.

There is a number of publications dealing with the evaluation of conversion factors, the most prominent among them are the paper of Adamiec and Aitken [12], its re-evaluation by Guerin, Mercier & Adamiec [7] [used in **ADELEv2017**] and the compilation by Liritzis et al. [13]. The latter shows that within the last two decades the published values scatter generally just by some per cent. Thus the differences between the recent sets of conversion factors are not the major sources of uncertainty in dosimetric age determination procedures.

2.2.2. Steps to a more realistic description of the system

Internal and external dose rate

The "*infinite dose rate*" $\dot{D}_\infty$ is just the first step to describe a real system. Normally, the radionuclide content of the dated object (grain, inclusion in ceramics, piece of a flintstone etc.) differs from that of the surrounding material (sediment, soil etc.). Thus one can calculate from these concentrations internal ($\dot{D}_{\infty,int}$) and external ($\dot{D}_{\infty,ext}$) "infinite dose rate" values for the object and the surrounding, respectively. These two values are generally not the same but represent the next step in determining the dose rate "seen" by the dated object.

It should be mentioned that the terms "internal" and "external" are not unambiguous: For a potsherd buried in soil "internal dose" is sometimes used for the contribution from the ceramics in contrast to the "external dose" from the soil. Hereafter in the text, the term "internal" will be strictly limited to that object which is actually subject of luminescence investigations. Let us assume that in the case cited above quartz inclusions in a thin potsherd of some mm thickness are dated e.g. by thermoluminescence. Since this ceramics does not attenuate γ radiation, the external γ dose rate originates only from the soil radioactivity whereas the α and β component of the external dose has to be calculated from the radioactivity of the ceramics itself. This procedure is a consequence of the short α and β ranges in ceramics. Artefacts or other buried objects should be treated as thin layers according to the sandwich geometry procedure described as a special case in chapter 2.3.2.

The next step in the calculation of the dose rate considers a system consisting of a "dirty" object containing radioactivity which is situated in a "clean" environment without radiation sources (illustrated by case **b)** in Figure 35). The dose rate deposited in the "dirty" object results only from the radionuclides inside. Compared to $\dot{D}_{\infty,int}$ it lacks the contribution of the

surrounding material acting on the investigated object. Therefore the real dose rate in the object $\dot{D}_{int}$ is smaller than $\dot{D}_{\infty,int}$. This fact is taken into account by the introduction of a correction term ϕ in the calculation of the *internal dose rate*:

$$\dot{D}^{i}_{int} = \phi^{i} \cdot \dot{D}^{i}_{\infty,int} \text{ with } i = \alpha, \beta \text{ and } \phi < 1 \quad \text{(Eq. 11)}$$

ϕ describes the fraction of the "infinite dose rate" which is absorbed by a "dirty" object of limited size. It depends on the ratio of its size to the range of the radiation and therefore on the dimension of the object (e.g. diameter of spherical inclusions or grains) as well as on type and energy of the radiation.

In general, the size of the objects is essentially smaller than the half value layers of the γ radiation and so the γ contribution to the internal dose rate is negligible (ϕ^{γ} = 0).

Complementary to this, the real contribution of the external radiation field to the embedded object is obtained if the system is approximated by the picture of a "clean" object in a "dirty" matrix (case **c)** in Figure 35). For this situation the dose rate is then that of the system in radiative equilibrium minus the sketched model "dirty" object in "clean" environment.

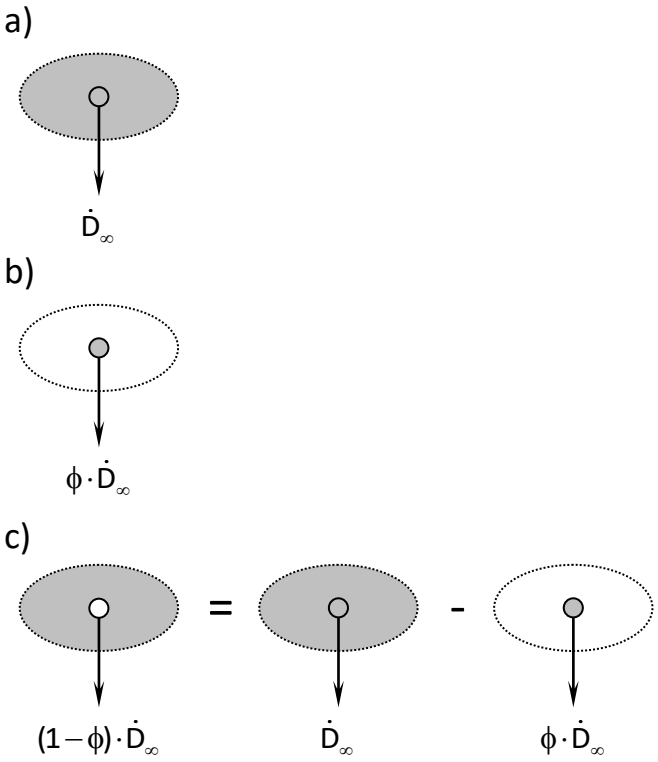

Figure 35 Illustration of the models used for the dose rate calculation in objects of limited sizes:
a) The object is part of the ideal, infinite, isotropic system with homogeneously distributed radiation sources. In this state of radiative equilibrium it receives the "infinite dose rate" $\dot{D}_{\infty}$.
b) Same radionuclide concentration as in a) but restricted to the "dirty" object in a "clean" environment free of radioactivity. The object absorbs only the fraction $\phi \cdot \dot{D}_{\infty}$ of the infinite dose rate. This model is used for the calculation of internal dose rates of grains or inclusions.
c) The opposite problem of a "clean" object in a "dirty" environment results from the difference of case a) and b). This approach is used for the

determination of the dose rate deposited in the object from external sources, the external dose rate.

Resulting from Figure 35 one finds for the real external dose rate in the object:

$$\dot{D}^{i}_{ext} = (1-\phi^{i})\cdot\dot{D}^{i}_{\infty,ext} \text{ with } i = \alpha, \beta, \gamma \quad . \text{(Eq. 12)}$$

Note that because of $\phi^{\gamma} = 0$ the external dose rate of the γ component does not differ from the infinite case.

The ϕ-factor concept can be applied to an additional problem. Heterogeneously distributed α emitter in the matrix and the very short α ranges may cause an inhomogeneous external α radiation field. Since the α dose deposition occurs only in the outer 20 µm of a mineral grain, etching of the surface layer is often applied during the preparation of coarse grain samples to remove the effect of inhomogeneity. This grain volume reduction necessitates a further correction of the actual grain dose. In this case ϕ becomes a function of the etched layer thickness in addition to its grain size dependency.

Values of correction factors for a large diameter range of spherical objects, for several etching layer thicknesses and both for the α and the β dose component from the ^{238}U and ^{232}Th decay series were already published in the early days of luminescence dating (see [14], [15] and [16]). In contrast to the approach shown above these papers discuss the fraction of the external dose absorbed in the dated object, i.e. they tabulate (1-ϕ) values. Monte Carlo procedures were used more recently to produce updated ϕ values (see [17] for the α dose component and [18] for β and γ [the data from these references were used in **ADELEv2017**]).

Results of the ϕ value simulation for the β dose from the total U decay series deposited in spherical quartz grains [18] are plotted in Figure 36.

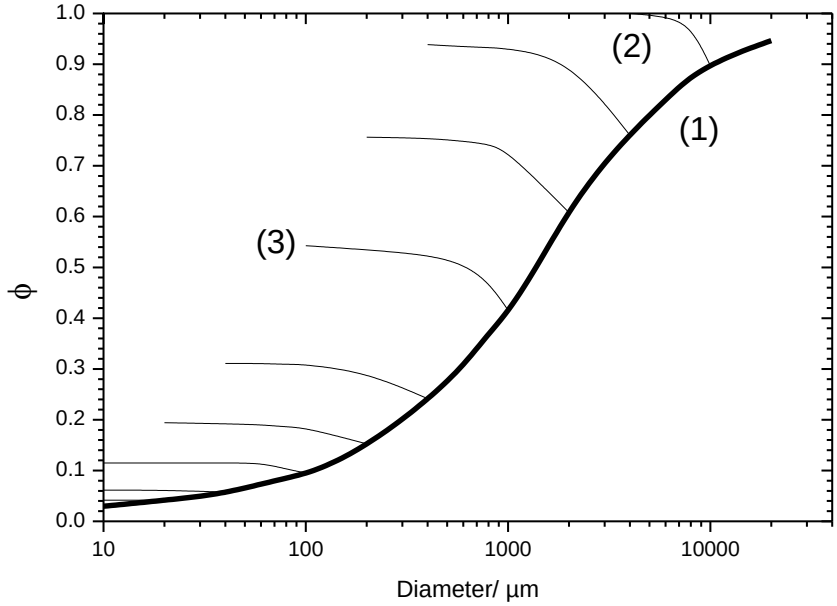

Figure 36 ϕ values for the β dose from the U decay series absorbed by spherical grains [18]. The numbers are explained in the text.

The strong line corresponds to the dose fraction in unetched grains, whereas the thin curves demonstrate the effect of consecutive etching starting from the unetched grain diameter. Some clearly visible characteristics of ϕ are marked in the plot:

(1) The deposited internal dose in unetched grains tends to zero for very fine grains and increases to 1 for large objects. This means, fine particles “see” mainly external dose components and are influenced only to a small extent by their own radionuclide content. Regarding the internal beta dose large “grains” (> 1 cm) on the other hand behave like systems of infinite extension; the dose leakage in their surface layer is negligible.

(2) Etching of large objects leads to a removal of this leakage layer. The remaining etched part is in radiative equilibrium (ϕ =1)

(3) Small grains do not include a region of radiative equilibrium. This is the case for all grains diameters smaller than the β ranges. Etching of those grains lead to a saturation value of ϕ but not to ϕ = 1.

Moisture correction

The next parameter which has to be involved into a realistic scenario for dose rate calculation is the moisture content of the material under investigation and of its surrounding. Compared to mineral grains water shows only very low concentrations of U, Th and K. Otherwise, it has the ability to attenuate the radiation field and hence to reduce the dose rate acting on the sample. According to [19] the *moisture corrected external dose rate* for the α, β and γ component is

$$\dot{D}^{\alpha}_{\infty,m} = \frac{\dot{D}^{\alpha}_{\infty}}{1+1.5\cdot M} \qquad \text{(Eq. 13)}$$

$$\dot{D}^{\beta}_{\infty,m} = \frac{\dot{D}^{\beta}_{\infty}}{1+1.25\cdot M} \qquad \text{(Eq. 14)}$$

$$\dot{D}^{\gamma}_{\infty,m} = \frac{\dot{D}^{\gamma}_{\infty}}{1+1.14\cdot M} \qquad \text{(Eq. 15)}$$

The *moisture* M is defined as the ratio of the water mass to the dry mass of the material

$$M = \frac{m_{H_2O}}{m_{dry}} \qquad \text{(Eq. 16)}$$

and may therefore vary from zero in a dry matrix to large values > 1 for light material with high water content (e.g. wet organic material like peat).

The effect of the moisture correction is demonstrated in Figure 37. Water contents of some ten percent already reduce the external dose to the same extent.

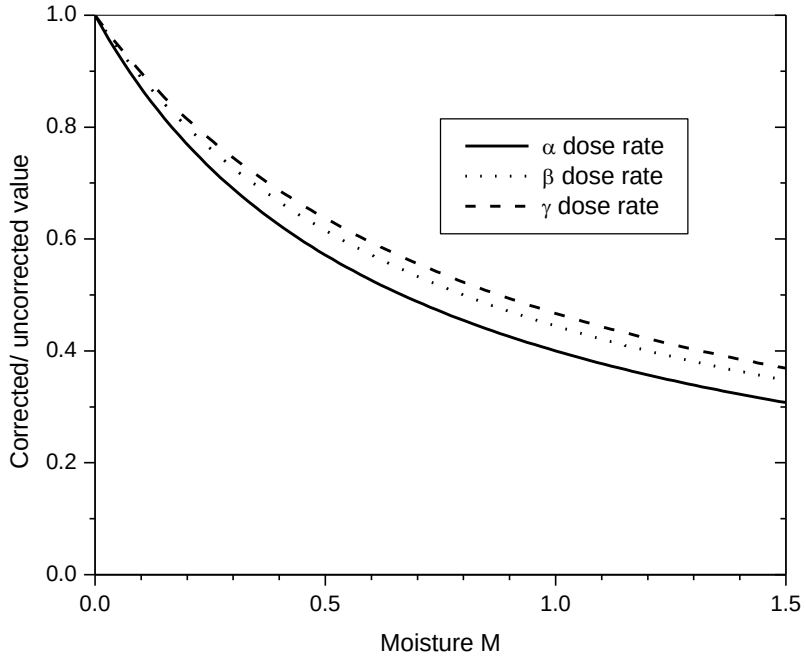

Figure 37 Effect of the correction on the uncorrected external dose rates.

Therefore a careful moisture determination is strongly recommended. Current values may not necessarily represent the mean water content in the past. A search for additional information is often necessary to get a reliable result. Especially the water saturation content should be determined to get an idea of the range of possible earlier moisture variations. The case of time dependent moisture contents is described in chapter 2.3.3

It should be mentioned that the external dose rate is attenuated by moisture prior to its partial deposition in the dated object. The *external dose rate* acting on the object is thus correctly calculated by

$$\dot{D}^{i}_{ext} = (1-\phi^{i}) \cdot \dot{D}^{i}_{\infty,ext,m} \text{ with } i = \alpha, \beta, \gamma \quad \text{(Eq. 17)}$$

where $\dot{D}^{i}_{\infty,ext,m}$ is determined as described before.

Density correction

Up to now it was assumed that the object under investigation shows the same composition as the ambient matrix material. This condition is not generally fulfilled, see the task of determining ϕ factors for feldspar grains from tabulated quartz values. The dosimetric properties can be simply translated if both materials possess the same mean atomic number $\overline{Z}$ but differ in their densities ρ like SiO_2 ($\overline{Z}$ = 10.0, ρ = 2.65 g cm^{-3}), K-feldspar ($\overline{Z}$ = 10.6, ρ = 2.58 g cm^{-3}) and $CaCO_3$ ($\overline{Z}$ = 10.0, ρ = 2.73 g cm^{-3}).

For these materials the stopping power values S(E) are equal, i.e. according to Eq. (8) the absorbed energy dE depends from the area density $\rho \cdot dx$ alone. Thus the energy deposition is the same for two objects of composition 1 and 2 along the thickness d_i when Eq. (18) is fulfilled:

$$d_1 = \frac{\rho_2}{\rho_1} \cdot d_2 \qquad \text{(Eq. 18)}$$

$d_{1,2}$ - typical dimension of material 1 or 2, resp.

$\rho_{1,2}$ - density of material 1 or 2, resp.

For instance, the energy absorption in 100 µm of K-feldspar is equivalent to 97 µm of quartz.

If d_i is a typical dimension of an object (e.g. the diameter of a spherical grain) it can be proved that two objects with the same mean atomic number but different densities ρ_1 and ρ_2 are dosimetrically identical if Eq. (18) is satisfied. With other words, every size dependent correction (like the ϕ factor) can be scaled by using this equation.

This conclusion does not hold for materials with different $\overline{Z}$ because of the Z-dependence of the secondary electrons production by ionising radiation.

2.2.3. Calculation of the total absorbed dose

Based on the preceding information one can now assemble the totally deposited dose rate starting from the radionuclide concentrations in the dated object and the environment. The internal dose $\dot{D}_{int}$ is determined according to Eq. (11) in consideration of grain size and etched surface layer thickness. The external dose is first corrected for moisture (Eqs. (13) to (15)) and then for size and etching Eq. (17). At last *total energy dose rates* $\dot{D}^{\alpha,\beta,\gamma}$ are derived as

$$\dot{D}^{i} = \dot{D}^{i}_{int} + \dot{D}^{i}_{ext} \text{ with } i = \alpha,\beta,\gamma \quad \text{(Eq. 19)}$$

At this point one should commemorate that the palaeodose, as deduced from the natural luminescence signal and the reconstructed dose response curve, is not identical to the total energy dose transferred from the radiation field to the luminescence sample. In chapter 2.1.1 the high energy density along alpha tracks was stated. This is associated with a saturation of the luminescence traps and results in a reduced luminescence yield compared to the impact of β or γ irradiation. This effect is also well known in other applications; e.g. in scintillators used for the detection of ionising radiation (NaI(Tl) crystals, organic cocktails for liquid scintillation counting, plastic scintillators etc.). Here the occurrence of a lower light yield for α particles compared to β or γ radiation is called “quenching” and leads to different energy calibration factors.

The lower efficiency of the real α dose is considered by an α efficiency factor a, sometimes called a-value. The *total effective dose rate* $\dot{D}^{eff}_{total}$ responsible for the detected luminescence signal is therefore not the simple sum of the energy dose rates but

$$\dot{D}^{eff}_{total} = a \cdot \dot{D}^{\alpha} + \dot{D}^{\beta} + \dot{D}^{\gamma} + \dot{D}^{cosmic} \quad \text{(Eq. 20)}$$

a - α-efficiency

Eq. (20) also includes the cosmic contribution $\dot{D}^{cosmic}$ whose determination is described in Chapter 2.1.2.

The $\dot{D}^{eff}_{total}$ is eventually used for the age calculation from the palaeodose D_P . Usually it is assumed that $\dot{D}^{eff}_{total}$ is constant with time and the luminescence age t_L becomes

$$t_L = \frac{D_P}{\dot{D}^{eff}_{total}} \qquad \text{(Eq. 21)}$$

Under a more general perspective the dose rate may vary with time and becomes time dependent. Examples for this are mentioned and exemplified in the following Chapter 2.3. The effective dose collected since the last bleaching of the luminescence signal is then

$$D^{eff}_{total} = \int_{t_b}^{t_b+t_L} \dot{D}^{eff}_{total}\, dt \quad \text{(Eq. 22)}$$

t_b - moment of the last bleaching event

With the knowledge of the palaeodose D_P, the determination of the luminescence age is equivalent to solving the integral equation (23) for t_L:

$$D_P = \int_{t_b}^{t_b+t_L} \dot{D}^{eff}_{total}\, dt \quad \text{(Eq. 23)}$$

An analytical solution is generally not practicable. Instead of this Eq. (23) has to be solved by an iterative procedure. Starting at the last moment of zeroing the luminescence signal t_b, the integral is summed up until it is equal to D_P. The time elapsed since the start is then the wanted age value t_L.

The complete sequence of luminescence age calculation starting from the radionuclide contents, the properties of the investigated objects, the sample preparation and the geographic position is summarised in Figure 38 to get an overview over this procedure.

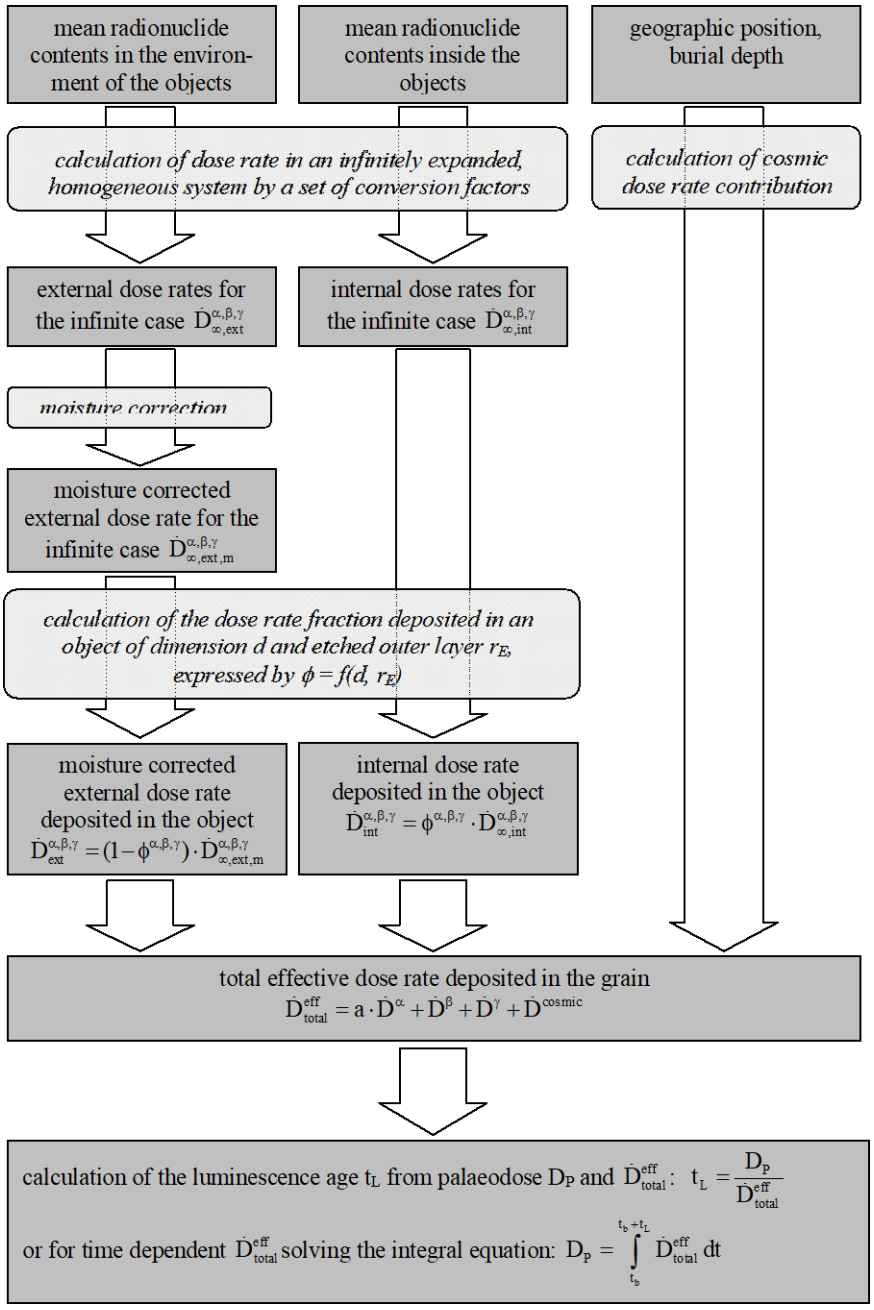

Figure 38 Overview of the calculation procedure for the dose applied during burial of the sample.

2.2.4. Typical examples

To get an impression about the influence of the different dose rate contributions for the dating of typical sediment systems, three simplified systems were defined (characterised in Table 3): in **Sediment I** and **II** luminescence dating was performed on coarse grained quartz and feldspar, respectively. The surrounding material was assumed to contain rather low specific activities of the ^{238}U and ^{232}Th decay series and ^{40}K as typically found in sandy deposits. **Sediment III** is rather clayey with higher levels of the surrounding radioactivity, the dated material is feldspar from the fine grained polymineralic fraction. These typical sediments will be also used in chapter 2.3 to illustrate the deviations caused by non-standard cases.

Sampling point:

Longitude	15° E
Latitude	50° N
Altitude	0 m
Cover	500 cm
Cover density	1,8 g cm^{-3}

Grain properties:

Type	Grain size [µm]	Material	Density [g cm^{-3}]	Etched layer [µm]	a-value
Sediment I	100 - 150	Quartz	2.65	10 ± 2	0.10 ± 0.02
Sediment II	100 - 150	Feldspar	2.55	10 ± 2	
Sediment III	7 - 10	Feldspar	2.55	-	

Type	Internal element content		
	U [ppm]	Th [ppm]	K [%]
Sediment I	0	0	0
Sediment II	0	0	12.5 ± 0.5
Sediment III	0	0	12.5 ± 0.5

Sediment properties:

Type	Specific activity [Bq kg^{-1}]			Moisture [%]	
	^{238}U series	^{232}Th series	^{40}K	current	saturation
Sediment I	10 ± 1	10 ± 1	150 ± 10	**5 ± 1**	**25 ± 5**
Sediment II	10 ± 1	10 ± 1	150 ± 10	**5 ± 1**	**25 ± 5**
Sediment III	50 ± 5	50 ± 5	500 ± 25	**15 ± 2**	**35 ± 5**

Table 3 Characteristics of the investigated typical dating systems.

The contributions of the different types of radiation to the external and the internal dose rate are summarised in Table 4. For the alpha component only the effective dose rate is shown (cf. chapter 2.2.3).

Type	Dose rate [µGy a^{-1}]							
	Cosmic	External			Internal			Total
		alpha eff.	beta	gamma	alpha eff.	beta	gamma	
Sediment I	115 ± 11	13 ± 4	488 ± 25	309 ± 16	0	0	0	920 ± 100
Sediment II	115 ± 11	15 ± 4	490 ± 25	309 ± 16	0	491 ± 21	0	1420 ± 150
Sediment III	115 ± 11	1430 ± 300	1830 ± 80	1230 ± 70	0	25 ± 1	0	4620 ± 560

Table 4 Dose rate contributions for the typical systems from Table 3.

In **Sediment I** - quartz coarse grains - the total dose rate originates exclusively from external radiation and the cosmic component. Internal sources are missing because zero concentrations of U, Th and K were assumed for the quartz grains. The dose rate is mainly

determined by the external beta and gamma component; the deposition of the alpha dose is clearly reduced by etching the outer shell of the quartz grains. The cosmic contribution still amounts to more than 10 % of the total dose rate.

In **Sediment II** - same system like case I but dated by K-feldspar coarse grains - about 35 % of the total dose originates from irradiation of the grains by their own potassium content. Therefore especially in low dose environments the determined age is very sensitive to incorrect K concentrations of the grains. An accurate potassium analysis of the investigated minerals is essential in this case. Far-red radiophosphorescence (RP) of feldspars can be used to determine their potassium concentration ([20], [21]). Far-red RP is emitted by feldspar grains only (at least not from quartz) and so contaminants are excluded to a wide extent. However, the need of determining the exact RP peak position requires a sensitive luminescence spectrometer. The peak maximum shifts from 710 nm to 740 nm if the K-concentration changes from 14 % to 0%

Both **Sediments I** and **II** are nearly unaffected by the α dose rate. Etching of the outer 10 µm layer of the grains and the low α efficiency of 0.10 results in a drastic reduction of that originally dominating dose component (see Table 2).

Sediment III - dating of feldspar fine grains - exhibits again a dominant external dose rate with contributions of the three radiation components in the same order of magnitude. The internal radioactivity of the grains can be neglected (< 1 %) due to the low ϕ factor for small grains (cf. Figure 36 and the subsequent discussion). Although the α dose rate is reduced because of the low α efficiency still one third of the total dose rate is supplied by this fraction. This fact demands for a homogeneous radionuclide distribution and requires a careful determination of the a-value.

It is noteworthy that for all three **Sediments I**, **II** and **III** 35 - 50 % of the total dose rate are a consequence of the external β radiation field. Besides the α component this fact causes a fundamental sensitivity of luminescence dating to inhomogeneities up to the mm scale.

Let us assume that the measured palaeodose amounts to (50 $\pm$ 5) Gy in each case. The age data as determined by **ADELEv2017** are:

Sediment I (54 $\pm$ 6) ka
Sediment II (35 $\pm$ 4) ka
Sediment III (10.8 $\pm$ 1.3) ka

and reflect clearly the influence of the different total dose rates.

One final remark: Samples are often dated simultaneously by luminescence methods in different ways, i.e. by variable grain fractions differing in size and / or mineral type. If these results do not agree, the reason is not necessarily an erroneous determination of the palaeodose. The different weighting of the single dose rate components may also result in such a phenomenon. This may occur inter alia if some of the parameters needed for the age calculation are not known exactly enough or if their time functions are unknown. In the following section will discuss especially the consideration of time dependent effects on the luminescence dating procedure.

2.3. Dose-rate determination: Non-standard cases

As indicated above, the dose rate is not necessarily constant over time. One of the following parameters may vary with time: thickness of the covering layer, moisture and radionuclide content in the environment. Then Eq. (21) is no more applicable and must be replaced by the integral equation (23). Consequences for the calculation of the age are discussed already there, in the following we will continue with some examples of the impact of such time dependent parameters.

It should be mentioned that all corrections described below have one important drawback in common: they are all based on assumptions about the system's history which cannot be fully verified nowadays. So, one should test different "reasonable" (i.e. in accordance with the presently observed status) models to get an impression about the spread of age results obtained by these models. The indication of the final result should reflect this model dependent variety of the age value.

2.3.1. Covering layer

The overburden of an artefact or a sediment sample is often assumed to be constant with time. In the light of the time periods covered by luminescence dating this precondition is rather the exception than the rule. Strong sedimentation as well as erosion results in variations of the covering thickness in the order of some meters. For systems showing a great contribution of the cosmic component to the total dose rate these processes may result in a growing uncertainty of the age result. This may be the case when

(i) the external and internal dose is low. Sediments rich in quartz sand often show specific activities of the ^{238}U and ^{232}Th chain clearly below 10 Bq kg^{-1} and ^{40}K activities < 100 Bq kg^{-1}. Then the external dose rate does not exceed some 100 µGy a^{-1} and is in the order of magnitude of the cosmic dose rate (cf. Figure 33). Low internal radionuclide contents enhance this effect; thus dating of quartz is more sensitive to changes of the cosmic dose rate than that of feldspar grains.

(ii) the dating sample was taken close to the present surface. At least currently the cosmic dose rate of some 100 µGy a^{-1} significantly influences the dating result. But this contribution may become insignificant if overburdens of more of some 10 cm were dominant in history and were eroded just recently.

(iii) the sample was taken at elevated altitudes. Whereas at sea level 45 cm overburden (ρ = 2 g cm^3) are enough to reduce the cosmic dose rate below 200 µGy a^{-1}, at 2000 m altitude 320 cm of covering sediment are necessary to achieve the same value. Dating of samples from mountain areas therefore require a careful consideration of the overburden's history.

Example:

The **Sediments I**, **II** and **III** defined in chapter 2.2.4, now covered by 500 cm of sediment, had an overburden of 100 cm until 7 ka B.P. and were buried thereafter by a heavy sedimentation event. Taking into account that the cosmic dose rate became time dependent by this event, the ages corrections for the variation of the cosmic dose rate are given in Table 5:

Type	Age/ ka	
	uncorrected	corrected
Sediment I	(54 ± 6)	(49 ± 5)
Sediment II	(35 ± 4)	(33 ± 4)
Sediment III	(10.8 ± 1.3)	(10.2 ± 1.2)

Table 5 Example for the effect of changing overburden on the dating results for the sediments defined in Table 3.

The age of **Sediment I** (coarse grained quartz) deviates most obviously (≈ 10 %) from the case of constant cosmic dose rate, indicating its sensitivity to even slight changes in the environmental conditions.

2.3.2. Layered geometry

One presumption of the previous considerations was the existence of a sample environment which is homogeneous at least at the scale of the typical range of γ-quanta in the material, e.g. in the order of several ten centimetres. This is not necessarily fulfilled e.g. for the finding situations of archaeological objects or for sediments deposited in sediment traps like lakes. Also a sherd found in a homogeneous environment is described by this model. In these situations abrupt variations in the activity concentrations may occur which cause stepwise changes in the gamma dose rates. Due to the distinctively lower ranges of α- or β-particles their dose rate distributions are generally not influenced.

The mathematical treatment of such layered situations in dose rate calculations is well described in [19] and should be just summarised here.

Let us start with considering the border between an inert layer (free of activity) and a material containing radionuclides. Both materials should be equal in all other parameters and infinitely expanded in each half space. Such an arrangement is shown in Figure 39.

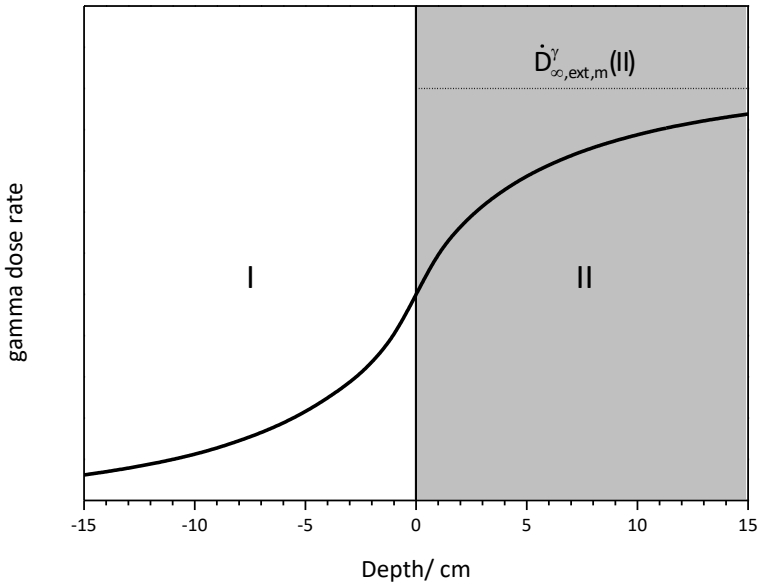

Figure 39 Gamma dose rate gradient at the border I | II between an inert layer I and a radionuclide containing layer II for which its "infinite", moisture corrected gamma dose rate $\dot{D}^{\gamma}_{\infty,ext,m}(II)$ is shown by the dotted line.

Near the transition I | II, the radiative equilibrium is no more conserved. The energy of gamma quanta emitted in layer II is not completely absorbed in this material, the nearer the transition the more is lost. At the edge only one half of $\dot{D}^{\gamma}_{\infty,ext,m}(II)$ is "seen" by a grain since solely the right half space contributes to the dose rate. A part of the radiation penetrates the inert layer I and causes the dose rate distribution to the left of the transition. Correction factors describing the gamma dose rate as a function of the distance from the discontinuity are listed in [19] for the U, Th and K content.

Knowing these factors, every discontinuity I | II between materials of specific activities a(I) and a(II), respectively, can be interpreted as a superposition of transitions to inert layers (here labeled as "0"):

$$I \mid II = I \mid 0 + 0 \mid II \quad \text{(Eq. 24)}$$

The case of a sandwich geometry of three systems I | II | III as occurring e.g. in layered sediments can be written also as a superposition of borders to inert material:

$$I \mid II \mid III = I \mid 0 \mid 0 + 0 \mid II \mid 0 + 0 \mid 0 \mid III \quad \text{(Eq. 25)}$$

with

$$0 \mid II \mid 0 = II \mid II \mid II - [II \mid 0 \mid 0 + 0 \mid 0 \mid II] \quad \text{(Eq. 26)}$$

II | II | II denotes the case of the homogeneous, infinitely expanded system II.

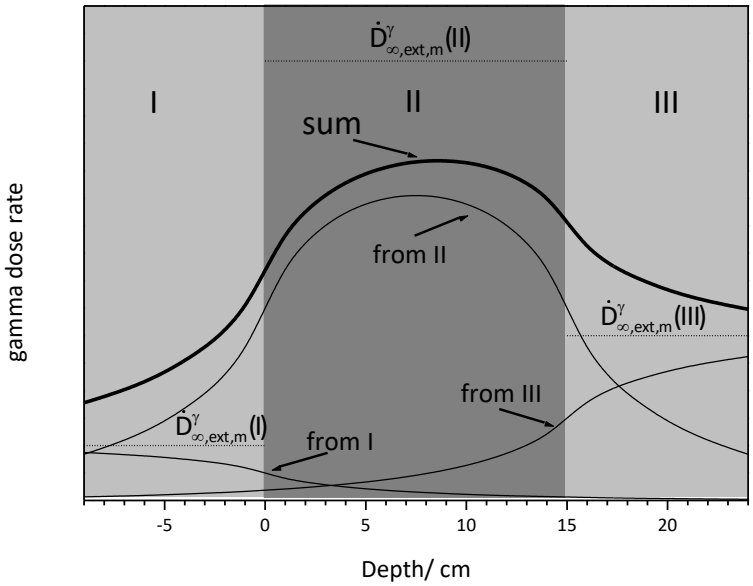

Figure 40 Gamma dose rate distribution in the layered system I | II | III. For each layer the "infinite", moisture corrected gamma dose rate $\dot{D}^{\gamma}_{\infty,ext,m}$ is shown as dotted line. The thin lines mark the dose rate contributions of the individual layers.

Figure 40 illustrates a case with a layered structure, showing the "infinite" external gamma dose rates for each layer as well as the contributions to the total external gamma dose rate. $\dot{D}^{\gamma}_{\infty,ext,m}(II)$ is not reached in layer II because of the limited extension of II, which is shorter than the characteristic penetration depth of gamma radiation. On the other hand the central layer influences on a scale of some 10 cm the dose rate in the adjacent material.

As a consequence, if sampling of material for luminescence dating near obvious discontinuities (e.g. an intermediary peat layer or a hiatus) cannot be avoided corrections must be carried out in the described way.

Example:

Again, the **Sediments I**, **II** and **III** from chapter 2.2.4 are used to illustrate the effect of a "sandwich" structure. Overlying and underlying layer shall contain organic material showing an U accumulation:

Overlying layer:

U	(100 ± 10) Bq / kg
Th	(5.0 ± 0.5) Bq / kg
K	(50 ± 5) Bq / kg
Moisture	(15 ± 5) %

Underlying layer:

U	(200 ± 20) Bq / kg
Th	(5.0 ± 0.5) Bq / kg
K	(50 ± 5) Bq / kg
Moisture	(15 ± 5) %

The thickness of the enclosed layer was 15 cm, the dating sample was taken at 5 cm below the upper layer boundary. In Table 6 the results of the correction for the layer geometry are listed.

Type	Age/ ka	
	uncorrected	corrected
Sediment I	(54 ± 6)	(41 ± 4)
Sediment II	(35 ± 4)	(29 ± 3)
Sediment III	(10.8 ± 1.3)	(10.9 ± 1.3)

Table 6 Example for the effect of layered geometry on the dating results for the sediments defined in Table 3.

Again, the age of **Sediment I** is most affected by the sandwich geometry (- 24 %) but also the dating of coarse grained feldspar in **Sediment II** is clearly influenced (- 17 %). About no effect is visible for the polymineralic fine grain fraction in **Sediment III**. It is explained by the a priori higher specific activities of this material and the dominance of the short range contributions from the alpha and beta radiation field which are unaffected by the layered geometry.

2.3.3. Moisture

The attenuating effect of moisture onto the external dose rate depends on the extent of pore filling by water. The upper limit is that of a moisture saturated system i.e. with all pores completely filled, the opposite limit is that of a dry system. Again, the “true” history of pore space filling is often a matter of speculation and can only be roughly approximated.

Even if the present moisture is low, it might have been much higher or yet saturated in the past, e.g. when the groundwater table was above the sample position during a more humid period. Such situations may occur in sediments from lakes or peat bogs, if changes between dry and humid periods occurred.

For good laboratory practice it is thus essential to determine both the present as well as the saturation moisture content.

Such a problem was modelled e.g. in reference [22] for a humic rich deposit. It was expected that during glacial times the conditions were much drier and that during these periods the sediment was not water saturated as today. The inclusion of a time dependent moisture level lead to age variations of about 10 % in comparison to the assumption of a constant moisture.

Example:

The effect of moisture variation was also tested on the model systems **Sediment I**, **II** and **III**. It was assumed that the material was saturated with water until at 100 a B.P. a water table drawdown occurred.

Type	Age/ ka	
	uncorrected	corrected
Sediment I	(54 ± 6)	(65 ± 7)
Sediment II	(35 ± 4)	(39 ± 4)
Sediment III	(10.8 ± 1.3)	(13.1 ± 1.6)

Table 7 Example for the effect of recently changed moisture on the dating results for the sediments defined in Table 3.

Considering this moisture change the ages for **Sediment I** (coarse grained quartz) as well as of **Sediment III** (polymineralic fine grains) are elevated by about 20 %. In both cases the external dose rate contributions are dominating (cf. Table 4). The unchanged internal dose rate reduces the correction effect to 11 % for **Sediment II**.

2.3.4. Radioactive disequilibria

As mentioned above (Chapter 2.1.1), the radionuclides ^{238}U, ^{235}U and ^{232}Th are the origins of radioactive decay series which pass instable isotopes of various elements until the chain stops at stable lead isotopes (remember Figure 30 and Figure 31)

Each decay series tends in closed systems towards a radioactive equilibrium, i.e. a state with equal production and decay rate (activity) for each member nuclide of one decay chain. This balance of activities becomes disturbed if one or more nuclides exchange with the environment.

The open system will then show *radioactive disequilibria*. If the degree of opening remains constant with time, the deviation from equilibrium will reach a steady state where the supply / removal rate is balanced by an increased / reduced activity of the exchanging nuclide (saturation). Furthermore its successors aspire an equilibrium with this saturation activity. The time constants for developing this secondary equilibrium are of the order of the half life of each nuclide - short living nuclides will follow the change faster than long living ones. Closing the system again has a similar effect: the disturbed chain link will recover the radioactive equilibrium at a time scale determined by its half life.

Radioactive disequilibria currently detected in the environment are therefore an indication of an open system or the aftereffect of a previous event.

(Note that the disturbance of the radioactive equilibrium may also be an side effect of sediment formation. If resulting in a closed system, the modern activity ratios may be utilised for dating techniques. A well-known example for such method is the ^{234}U / ^{230}Th dating of organic sediments like peat.)

The time dependence of several activities in the decay chains requires the application of the integration technique mentioned above for the calculation of the absorbed radiation dose during burial (cf. Eq. (23)). This calls in the strict sense for a precise knowledge of any relevant exchange process in the past. Since it is virtually impossible to satisfy this demand, one has to manage this situation with the examination of borderline cases representing preferably high and low mean dose rates in the past, respectively. The only constraints of this approach are that the constructed histories are reasonable, i.e. consistent with geological, geochemical and physical parameters of the system as well as with experiences on recent formations and that they are in agreement with the measured modern activity

values and ratios. The result is therefore only the specification of a time range between an upper and a lower limit age, corresponding to the low and the high mean dose case, respectively.

Numerous examples for the treatment of radioactive disequilibria in dating problems can be found in literature, among them the papers by Krbetschek et al. [23], Prescott and Hutton [24] and Olley et al. [25, 26] summarise the principal cases. A comprehensive presentation of origin, detection and application of radioactive disequilibria in the geosciences gives the monograph edited by Ivanovich and Harmon [27].

Mathematical treatment

The mathematical treatment of the evolution of radioactive disequilibria is described in detail in [28]. Here we will briefly summarise these findings.

Everything starts with coupled differential equations resulting from the definition of activity given in Eq. (1) The total rate of variation of the number of nuclei for one nuclide consists of a feeding ("+") and a discharging ("-") term which are related to the activity of the preceding and the observed nuclide in the decay series plus a term describing any possible exchange in an open system:

$$\begin{aligned}\frac{dN_i(t)}{dt} &= \left.\frac{dN_i(t)}{dt}\right|_{+} + \left.\frac{dN_i(t)}{dt}\right|_{-} \\ &= A_{i-1}(t) + A_i(t) + R_i(t) \qquad \text{(Eq. 27)} \\ &= \lambda_{i-1} \cdot N_{i-1}(t) + \lambda_i \cdot N_i(t) + R_i(t)\end{aligned}$$

$N_i(t)$ - time dependent number of nuclei of nuclide i in the decay series,

t - time (t < 0 past, t > 0 future),

$A_{i-1}(t)$ - activity of the precessor of nuclide i in the decay series,

$A_i(t)$ - activity of nuclide i in the decay series,

$R_i(t)$ - exchange rate of nuclei of nuclide i.

λ_{i-1}, λ_i - decay constant of nuclide i-1 (precessor) and nuclide i, respectively

The term R_i may be positive or negative, in closed systems it is equal to zero. Activity $A_{i-1}(t)$ is zero for the starting nuclide of the decay chain (i = 1). The set of equations (27) for a whole decay series can be analytically solved for certain types of geological systems. Among them are some cases of geological importance and relevance:

(1) Closed systems without any mass transfer to the environment ($R_i(t) = 0$); the present activity ratios are directly coupled to their initial values during the formation of the object.

(2) Open systems with supply/discharge of one or more radionuclides from the decay series; the amount $R_i(t)$ is constant in time. For clearity, the parameter $Q_i = \lambda_i \cdot R_i$ is used in the following; it describes the addition/loss of activity per time i.e. the activity exchange rate.

(3) Open systems with supply/discharge of one or more radionuclides from the decay series; the rate $R_i(t)$ is proportional to the number of nuclei of type i, i.e. $R_i = c_i \cdot N_i$. For the sake of simplicity, in the following the parameter $p_i = \frac{\lambda_i}{\lambda_i - c_i}$ is used in the formulae. For a supply or a discharge of nuclide i, c_i is > 0 or < 0 and thus p_i becomes > 1 or < 1, respectively. The

meaning of p_i is the ratio of the activities with to without radionuclide exchange in the stationary case.

For each of these examples the mathematical term describing the activity evolution can be written as a sum of exponential decays where t_o denotes the present, i.e. the moment of activity measurement:

for (1)

$$A_i(t) = \sum_{j=1}^{i} b_{ij} \cdot e^{-\lambda_j (t-t_0)} \quad \text{(Eq. 28)}$$

$$\text{with } b_{ij} = \frac{\lambda_i}{\lambda_i - \lambda_j} \cdot b_{(i-1)j} \ \forall j < i,\ b_{ii} = A_i(t_0) - \sum_{j=1}^{i-1} b_{ij} \quad \text{(Eq. 29)}$$

for (2)

$$A_i(t) = \sum_{j=1}^{i} \left(\frac{Q_j}{\lambda_j} + b_{ij} \cdot e^{-\lambda_j (t-t_0)} \right) \quad \text{(Eq. 30)}$$

$$\text{with } b_{ij} = \frac{\lambda_i}{\lambda_i - \lambda_j} \cdot b_{(i-1)j} \ \forall j < i,\ b_{ii} = A_i(t_0) - \sum_{j=1}^{i} \frac{Q_j}{\lambda_j} - \sum_{j=1}^{i-1} b_{ij} \quad \text{(Eq. 31)}$$

for (3)

$$A_i(t) = \sum_{j=1}^{i} b_{ij} \cdot e^{-\frac{\lambda_j}{p_j} (t-t_0)} \quad \text{(Eq. 32)}$$

$$\text{with } b_{ij} = \frac{\lambda_i}{\frac{\lambda_i}{p_i} - \frac{\lambda_j}{p_j}} \cdot b_{(i-1)j} \ \forall j < i,\ b_{ii} = A_i(t_0) - \sum_{j=1}^{i-1} b_{ij} \quad \text{(Eq. 33)}$$

i, j	-	indices describing the nuclide
A_i	-	activity of nuclide i
b_{ij}	-	matrix elements referring to nuclide i and j, respectively
λ_i	-	decay constant of nuclide i
t	-	time
t_0	-	start, i.e. moment of burial
Q_i	-	activity exchange rate of nuclide i (s. above)
p_i	-	parameter for exchange of nuclide i proportional to the number of nuclei (s. above)

Some features of Eqs. (28) to (33) are obvious:

- The activity time function of each nuclide includes contributions of all precursors in the decay series.

- In the case of constant exchange rates Q_i (Eq. 30), the activities are shifted by a value of $\frac{Q_i}{\lambda_i}$ compared to the closed system case; for long time periods this leads to a shift of the steady state activities.

- In the case of an exchange proportional to the existing number of nuclei (Eq. 32) the parameters p_i act like modifications of the decay constant (or of the half life)

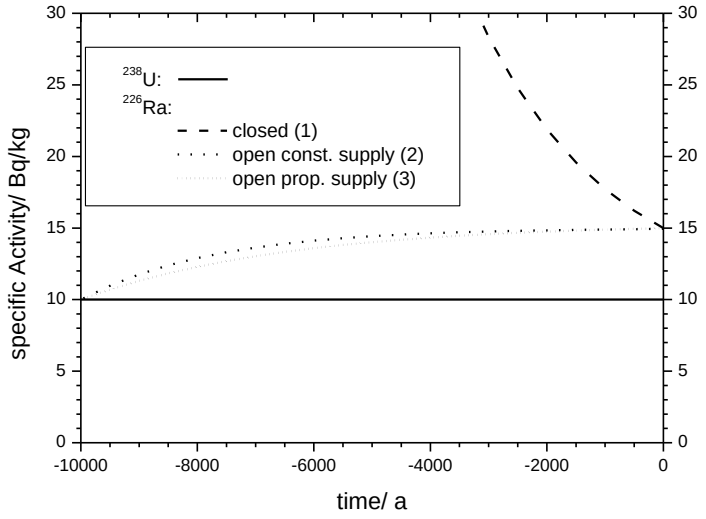

Figure 41 Plot of different activity models for a sample with a modern ^{238}U / ^{226}Ra disequilibrium (at time t = 0). For the different models, the numbers in brackets belong to the cases described above.

Figure 41 illustrates the three cases by an uncomplex fictional example: The modern activities (at time t = 0) of ^{238}U and ^{226}Ra were found to be 10 Bq/ kg and 15 Bq/ kg, respectively. There is evidence of an undisturbed equilibrium in the sample from ^{238}U to ^{230}Th. For some reasons, in the open systems started a Ra supply 10,000 a before today.

For the closed system (case 1), the ^{226}Ra excess over ^{238}U has to decline with time according to its half life of 1600 a. It will asymptotically converge to the ^{238}U activity, which is virtually constant in time. In the past the ^{226}Ra excess increases strongly with time, so for "reasonable" conditions (i.e. realistic ^{226}Ra activities) the moment of closing the system is limited to some thousand years before today.

An open system with a constant activity input rate $Q_{Ra\text{-}226}$ for ^{226}Ra (case 2) shows an asymptotic behaviour towards an ^{226}Ra equilibrium activity larger than the ^{238}U activity. The convergence to the limiting value is determined by the half life of ^{226}Ra, i.e. the difference to the limit is halved every 1600 years. After 10,000 a (the viewed interval) the ^{226}Ra activity is thus close to the asymptote. The asymptote is shifted by $\frac{Q_{Ra-226}}{\lambda_{Ra-226}} = 5.0\ \mathrm{Bq \cdot kg^{-1}}$ compared to the equilibrium case, i.e. the activity supply rate for ^{226}Ra is $Q_{Ra\text{-}226} = 2.17\ \mathrm{mBq \cdot kg^{-1} \cdot a^{-1}}$.

In case (3) the activity-proportional term $p_{Ra\text{-}226}$ = 1.5 results in a retardation of the asymptotic behaviour like it would occur for a nuclide with the half life $T_{1/2}$ = 1.5 ·1600 a = 2400 a. Factor p also describes the ratio of the ^{226}Ra to the ^{238}U activity in the steady state, as almost reached after 10,000a.

All cases mentioned have in common a time constant controlled by the half life of the "disturbed" nuclide. It reflects the general rule in the consideration of radioactive disequilibria:

Regardless the type of the system, any decay series will tend asymptotically to a new equilibrium state. The time constant necessary to "anneal" the disturbance depends on the half life of the affected nuclide and is in most cases equal to it.

A consequence of this rule is that in the majority of cases only the ^{238}U decay series will be examined for radioactive disequilibria. According to Figure 31 in the ^{232}Th decay series the longest half life except that of ^{232}Th itself is that of ^{228}Ra with 5.7 a. Thus, disequilibria either do not occur in the ^{232}Th series or are the result of short term variations in open systems whose course in past times are very uncertain. ^{232}Th series disequilibria are therefore usually not considered.

Furthermore, the little contribution of the ^{235}U series to the total dose rate (< 5 %) is reason for neglecting investigations on disequilibria in that chain.

Reasons for radioactive disequilibria

The risk for a member of a decay series to cause a radioactive disequilibrium depends on its ability to interact with the environment and on its affinity to chemical or physical differentiation processes.

A basic parameter ruling the capability of one nuclide to be exchanged by chemical processes is its half life. In an equilibrium state of the decay series (equal activities) the number of nuclei belonging to a certain chain member is proportional to its half life (cf. Eq. 1 and 3). So a short living nuclide has not only less time to interact with the environment, it is also less concentrated compared to a longer living one. The consequence is a higher probability for long living isotopes to undergo chemical reactions and thus to be exchanged with the surroundings. Similar statements are valid for physical processes. An example is the degree of radon (^{222}Rn) exhalation in soil which mainly depends on the mean diffusion path length of radon during its lifetime.

Decay series	Nuclide	Half life	Significant Properties
^{238}U series	^{238}U	$4.5 \cdot 10^{9}$ a	Actinide, heavy metal, forms organic complexes, valence states U(IV) (low solubility) and U(VI) (soluble as uranyl ion $(UO_2)^{2+}$)
	^{234}U	$2.5 \cdot 10^{3}$ a	
	^{230}Th	$7.4 \cdot 10^{4}$ a	Actinide, tetravalent, low solubility
	^{226}Ra	$1.6 \cdot 10^{3}$ a	Earth alkali metal, soluble
	^{222}Rn	3.8 d	Inert gas
	^{210}Pb	$2.2 \cdot 10^{1}$ a	Heavy metal, forms organic complexes
^{232}Th series	^{232}Th	$1.4 \cdot 10^{10}$ a	cf. ^{230}Th
	^{228}Ra	5.8 a	cf. ^{226}Ra
	^{228}Th	1.9 a	cf. ^{230}Th

Table 8 Physical and chemical properties of nuclides from the main decay series which may be responsible for radioactive disequilibria.

Table 8 summarises some general physical and chemical properties of mostly long living isotopes whose combination give rise to differentiation processes resulting in radioactive disequilibria. For instance, freshwater lakes will contain higher concentrations of dissolved Uranium than of Thorium. Organic material tends to bind Uranium by complexation, especially under anaerobic conditions. A lake sediment then may contain a mineralic detritus showing radioactive equilibrium plus an organic fraction enriched in Uranium but depleted in Thorium. ^{238,234}U / ^{230}Th disequilibria are common characteristics of limnic sediments, but for a dosimetric simulation one has to decide if the observed system is a close or an open one.

Other typical candidates for radioactive imbalances are: every organic material like peat, layers exposed to fluctuating groundwater levels, carbonate containing material (especially with remnants of mussel shells or corals) and remnants of metallurgical processes like slags. Here disequilibria can also occur and it is advisable to check for them as a precaution.

Note that deviations of ^{210}Pb from the rest of the series are common in near-surface soil horizons. Generally, the highest layers show a distinct ^{210}Pb excess over ^{226}Ra due to atmospheric supply of ^{222}Rn successors. The organic soil horizons are especially subject to such accumulations since Pb tends to form complexes with organic matter (cf. Table 8).

Consequences of radioactive disequilibria for dating

The next point is to illustrate the consequences of radioactive imbalances on dating results of our standard systems. For the sake of clearness we will concentrate on the polymineralic fine grain system **Sediment III**.

Under the assumption of an equilibrated decay chain the γ-spectrometrically determined specific activity of ^{226}Ra is frequently used as that of the whole series. Let us assume that the value given in Table 3 for the ^{238}U decay series [(50 ± 5) Bq kg^{-1}] actually is that of ^{226}Ra and that a more in-depth analysis additionally provided true ^{238}U values. Unfortunately, because of its low intensity γ-peak, ^{230}Th was below detection limit. Let us consider the following cases depending on the U results and discuss for their possible reasons:

- **Example 1**: today an obvious U-excess is found: ^{238}U – 300 Bq / kg, ^{226}Ra – 50 Bq / kg
  - Reason I: One concludes from the geological situation that the system is closed since deposition. The U / Ra ratio points to an initial excess or depletion of one nuclide. One possibility is an equilibrium in the series from ^{238}U to ^{230}Th on the one hand and from ^{226}Ra on a lower activity level on the other hand. This model would necessitate the start just some hundred years before. The period is so short because within one half life (1600 a) ^{226}Ra would reach already half the activity of its precursors. Together with the other parameters the determined palaeodose cannot be absorbed within this period. This model is hence senseless.
  - Reason II: The system is closed as before but with an equilibrium only from ^{238}U to ^{234}U. Such a model would start with a ^{234}U / ^{230}Th disequilibrium as found usually in organic sediments sealed by clayey layers (see before). ^{230}Th and its followers restore the equilibrium on a timescale of its half life of 75,000 a. A compatibility with all other unmodified standard parameters (including palaeodose) is only achieved when the history of the sediment starts 7700 a before present at the activity levels ^{238}U...^{234}U – 300 Bq / kg, ^{230}Th... – 37 Bq / kg. The activity history plot is displayed in Figure 42 a), the dating result is outlined in Table 9.
  - Reason III: The sampled sediment shows debris of admixed calcareous shells. It was also found to be water-bearing which gave cause for the assumption of an Uranium uptake during burial. In this model a constant U-uptake rate was assumed. There exists only one well-defined history which starts 9100 a before and leads to the given palaeodose as well as to the present radionuclide contents. In this model the $^{238,234}U$ uptake rate is Q = 28.2 mBq / kg / a [Figure 42 b) and Table 9].
  - Reason IV: There is some hint that Ra was removed from the open system over the entire dated period. For instance, the material was sampled in an aquifer with continuous flow along a hillslope and showed strong bleaching marks or an excess of relocated Ra was found not far away at a tight clay layer. Chemical exchange processes depend on the concentration of an element so we apply the model of a ^{226}Ra removal rate proportional to the available ^{226}Ra content. After deposition the ^{226}Ra activity falls within a few thousand years to the modern diminished saturation value [cf. Figure 42 c)]. Thus the parameter p from Eqs. 32 and 33 is given by the current ^{226}Ra / ^{238}U ratio of 0.167.
  - Reason V: The behaviour as in the case described just before is reasonable and supported by some findings; but, the start of Ra discharge was more recently and associated e.g. with the construction of a trench or with lowering of the groundwater table. In this case the ^{226}Ra activity did not reach the steady state yet and p must be smaller than 0.167 [see Figure 42 c)].
- **Example 2:** Even in the case that no difference between ^{238}U and ^{226}Ra activity was found, it is possible that a disequilibrium arises because of emanation of the noble gas isotope ^{222}Rn from the investigated layer. One reason could be a larger porosity in adjacent regions or the proximity of an air filled cavity. This loss is only verifiable by a deficit of the longer living ^{222}Rn daughter ^{210}Pb. In our example a Rn leakage of 40 % (p = 0.6) would slightly increase the calculated age by about 10 % (Table 9)

a)

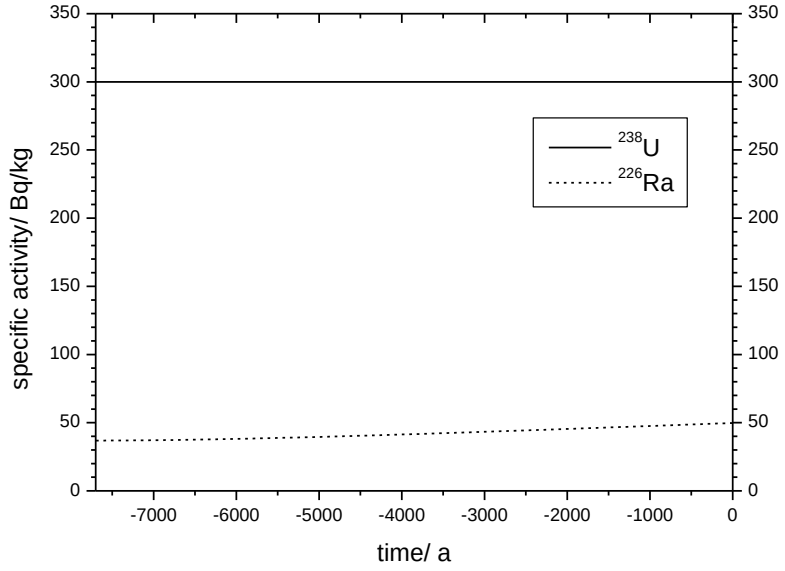
specific activity/ Bq/kg
time/ a
238U
226Ra
350
300
250
200
150
100
50
0
-7000
-6000
-5000
-4000
-3000
-2000
-1000
0

b)

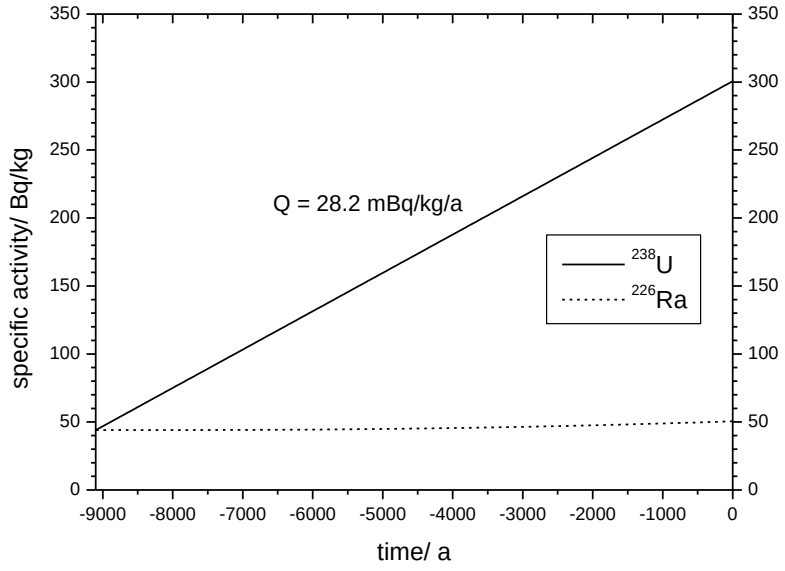
specific activity/ Bq/kg
time/ a
Q = 28.2 mBq/kg/a
238U
226Ra
350
300
250
200
150
100
50
0
-9000
-8000
-7000
-6000
-5000
-4000
-3000
-2000
-1000
0

c)

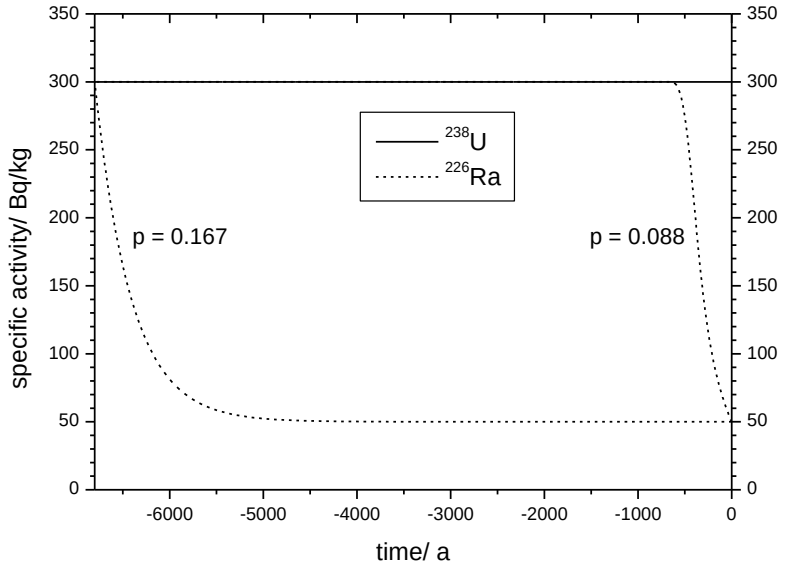

Figure 42 a) – c) Activity evolutions within the ^{238}U decay series in the past for the investigated system. Only the time functions of ^{238}U and ^{226}Ra are shown. The individual plots belong to different cases described in the text:
a) above – closed system with ^{234}U / ^{230}Th disequilibrium,
b) middle – open system with constant U uptake
c) below – continuous loss of ^{226}Ra starting at sediment deposition and 500 a before present, respectively.

System type	Modern activity	Characteristics	Age/ ka
closed	^{238}U 50 Bq/kg ^{230}Th not analysed ^{226}Ra 50 Bq/kg	undisturbed	**10.8 ± 1.4**
closed	^{238}U 300 Bq/kg ^{230}Th not analysed ^{226}Ra 50 Bq/kg	$^{234}U/^{230}Th$ disequilibrium	**7.7 ± 1.0**
open	^{238}U 300 Bq/kg ^{230}Th not analysed ^{226}Ra 50 Bq/kg	constant ^{238}U uptake, Q = 28.8 mBq/kg/a	**9.1 ± 1.1**
		permanent Ra loss, p = 0.167	**6.8 ± 0.9**
		permanent Ra loss since 500a, p = 0.088	**4.0 ± 0.5**
open	^{238}U 50 Bq/kg ^{230}Th not analysed ^{226}Ra 50 Bq/kg	permanent Rn loss, p = 0.6	**11.9 ± 1.4**

Table 9 Dating results for the standard system dated at the polymineralic fine grain fraction and with modern radioactive disequilibria in the ^{238}U decay series. The cases are described more in detail in the text.

The strong divergence of the age data found for these cases illustrate the imperative for a careful selection of the applied model and of the assumptions included. Furthermore it was shown that the choice of the applied model strongly depends on the amount of information about the material and the situation. One of this information is the preferably complete analysis of all long living radionuclides in suspicious systems. The used analytical method should therefore be adjusted to the complexity of the dated object.

Note

*The tutorial describes the approach applied for the software **ADELEv2017**. It is not an overview of the present state of art in the theory of dosimetry.*

References:

[1] Degering, D., Kulig, G., Krbetschek, M.: *ADELE* - a novel software for *A*ge *DE*termination based on *L*uminescence and *E*lectron spin resonance, Poster 11th Conference on Luminescence and Electron Spin Resonance Dating, Cologne, Germany, 24–29 July 2005

[2] Kulig, G.: Erstellung einer Auswertesoftware zur Altersbestimmung mittels Lumineszenzverfahren unter spezieller Berücksichtigung des Einflusses radioaktiver Ungleichgewichte in der ^{238}U-Zerfallsreihe, Bachelor thesis TU Bergakademie Freiberg, 2005

[3] Nucléide - Lara, Library for gamma and alpha emissions; http://www.nucleide.org/Laraweb/

[4] SRIM - The Stopping and Range of Ions in Matter; http://www.srim.org/

[5] NIST (National Institute of Standards and Technology) estar - stopping power and range tables for electrons; http://physics.nist.gov/PhysRefData/Star/Text/ESTAR.html

[6] Wedepohl, K.H.: The composition of the continental crust. Geochim. Cosmochim. Acta 59 (1995) 1217 - 1232.

[7] Guerin, G., Mercier, N., Adamiec, G.: Dose-rate conversion factors: update. Ancient TL 29 (2011) 5 - 8.

[8] Heusser, G.: Low-Radioactivity Background Techniques. Ann. Rev. Nucl. Part. Sci. 45 (1995) 543-589.

[9] Prescott, J.R., Stephan, L.G.: The contribution of cosmic radiation to the environmental dose for thermoluminescence dating. PACT 6 (1982) 17 - 25.

[10] Prescott, J.R., Hutton, J.T.: Cosmic ray and gamma ray dosimetry for TL and ESR. Nucl. Tracks Radiat. Meas. 14 (1988) 223 - 227.

[11] Prescott, J.R., Hutton, J.T.: The cosmic ray contribution to dose rates for luminescence and ESR dating: Large depths and long-term variations. Radiation Measurements 23 (1994) 497 - 500.

[12] Adamiec, G., Aitken, M.: Dose-rate conversion factors: update. Ancient TL 16 (1998) 37-50.

[13] Liritzis, I. et al.: A re-evaluation of radiation dose-rate conversion factors. Mediterranean Archaeology and Archaeometry 13 (2013) 1 - 15.

[14] Mejdahl, V.: Thermoluminescence dating: Beta-dose attenuation in quartz grains. Archaeometry 21 (1979) 61 - 72.

[15] Bell, W.T.: Attenuation factors for the absorbed radiation dose in quartz inclusions for thermoluminescence dating. Ancient TL 8 (1979) 2 - 13.

[16] Bell, W.T.: Alpha dose attenuation in quartz grains for thermolumines-cence dating. Ancient TL 12 (1980) 4 - 8.

[17] Brennan, B.J., Lyons, R.G., Phillips, S.W.: Attenuation of alpha particle track dose for spherical grains. Nucl. Tracks Radiat. Meas. 18 (1991) 249 - 253.

[18] Brennan, B.J.: Beta doses to spherical grains. Rad. Meas. 37 (2003) 299 - 303.

[19] Aitken, M.J.: Thermoluminescence Dating. Academic Press, London 1985.

[20] Dütsch, C., Krbetschek, M.R.: New methods for a better K-40 internal dose rate determination. Radiation Measurements 27 (1997), 377-381.

[21] Krbetschek, M.R., Goetze. J, Irmer, G., Rieser, U. and Trautmann, T.: The red luminescence emission of feldspar and its wavelenght dependence on K, Na, Ca-composition. Mineralogy and Petrology 76 (2002), 167-177.
[22] Preusser, F., Degering, D.: Luminescence dating of the Niederweningen mammoth site, Switzerland. Quaternary International 164–165 (2007), 106–112.
[23] Krbetschek, M.R., Rieser, U., Zöller, L., Heinicke, J.: Radioactive disequilibria in palaeodosimetric dating of sediments. Radiation Measurements 23 (1994), 485-489.
[24] Prescott, J.R., Hutton, J.T.: Environmental dose rates and radioactive dise-quilibrium from some Australian luminescence dating sites. Quaternary Science Reviews (Quaternary Geochronology) 14 (1995), 439-448.
[25] Olley, J.M., Murray, A., Roberts, R.G.: The effects of disequilibria in the uranium and thorium decay chains on burial dose rates in fluvial sedi-ments. Quaternary Science Reviews (Quaternary Geochronology) 15 (1996), 751-760.
[26] Olley, J.M., Roberts, R.G., Murray, A.S.: Disequilibria in the uranium decay series in sedimentary deposits at Allen's Cave, Nullarbor Plain, Australia: Implications for dose rate determinations. Radiation Measurements 27 (1997), 433-443.
[27] Ivanovich, M., Harmon, R.S. (eds.): Uranium Series Disequilibrium Applications to Environmental Problems. University Press, Oxford 1992.
[28] Degering, D., Köhler, M.: Gamma-spectrometric analysis of high salinity fluids – how to analyze radionuclides of the thorium decay chain far from radioactive equilibrium?, Appl. Radiat. Isot. 69 (2011) 1613 - 1617.